photonics

MDPI

Review

Versatile Meta-Devices: Principles and Applications

Hong Zhang, Zhangyi Du, Yitian Zuo, Yajie Huang, Jinkang Wu, Zhinuo Chen, Yifei Gao, Junbao Hu and Yu Lei *

School of Microelectronics and Data Science, Anhui University of Technology, Ma'anshan 243002, China; zhang_hong_25@163.com (H.Z.)
* Correspondence: leiyu@ahut.edu.cn

Abstract

Precise sculpturing of light empowers light with abundant phenomena across fundamental physics and practical applications. The emergence of metasurfaces provides a pivotal solution to the limitations of traditional optical components, which make it difficult to meet the integration requirements of diverse applications, and they are distinguished by their ultra-thin profiles, low optical losses, and high degree of controllability. In this paper, we elucidate the core physical principles to manipulate phase, amplitude, and polarization with meta-optic architecture, along with nonlocal effects. Specifically, we revisit the research progress and typical applications of meta-waveguides, meta-fibers, meta-lasers, meta-spectrometers, and meta-sensing. Finally, it looks forward to the future development direction of meta-optics in exploring the limits of light field control, chip-scale functional integration, and discovering new physical effects, providing theoretical and technical references for the development of metaphotonic devices.

Keywords: metasurface; meta-waveguides; meta-fibers; meta-lasers; meta-spectrometers; meta-sensing

1. Introduction

Light carries multidimensional information that can be perceived by human vision and analyzed by devices. Achieving flexible and precise control over light beams has always been a core pursuit in optical research. Based on the Huygens–Fresnel principle, the effective construction and modulation of optical wavefronts constitute the physical basis of beam manipulation [1–6]. By manipulating the fundamental properties of light waves, namely phase, amplitude, and polarization state, efficient conversion of information and energy can be achieved during the interaction between light and matter.

Traditional optical components rely on the phase accumulated during light propagation within a medium to achieve wavefront shaping. Their controllability is limited by classical laws of refraction and reflection and the intrinsic properties of materials, resulting in bulky optical systems that cannot meet the development of on-chip integration and multifunctional photonic chips [7–9]. In the last two decades, the emergence of subwavelength artificial structures, or metamaterials, has provided a new paradigm for overcoming the limitations of traditional optics.

Very recently, two-dimensional metamaterials, namely metasurfaces composed of subwavelength structural units, have driven the evolution of optical components towards ultrathinness, lightweighting, and multifunctional integration. Compared to three-dimensional metamaterials, metasurfaces offer significant advantages such as simple fabrication processes and compatibility with CMOS technologies, enabling highly flexible manipulation

Check for updates

Received: 1 April 2026
Revised: 17 April 2026
Accepted: 23 April 2026
Published: 28 April 2026

Copyright: © 2026 by the authors. Licensee MDPI, Basel, Switzerland. This article is an open access article distributed under the terms and conditions of the Creative Commons Attribution (CC BY) license.

of the incident light wavefront using planar configurations [10–15]. The physical mechanism of metasurfaces is not based on the traditional refraction effect but rather on the customized design of the scattering characteristics of subwavelength resonant units [16]. Early research mainly focused on metallic metasurfaces, utilizing plasmon resonance to enhance light-matter interactions, but ohmic losses limited their practical efficiency [17]. All-dielectric metasurfaces, with their low-loss and high-efficiency characteristics, have opened up new pathways for the realization of high-performance meta-devices [18,19].

The field of meta-optics has moved from fundamental physics research to the application of functional devices. Ultrathin optical elements based on metasurfaces have shown the potential to replace traditional optical systems, providing a feasible solution for on-chip integration and multi-dimensional parallel light-field manipulation [20,21]. All-dielectric metalenses, as a typical representative of meta-devices, integrate high numerical aperture, planar integration, and multi-dimensional light-field manipulation capabilities [22–24]. Meta-optics is expanding from single applications of light field manipulation and imaging to the field of optical computing based on wavefront operations. By performing mathematical operations such as spatial differentiation and convolution on light fields through metasurfaces, it provides a new paradigm for ultrafast analog optical computing [25–28].

With the deepening research on the physical mechanisms of metasurfaces and metamaterials, and the development of vector light field manipulation technology, meta-optics is gradually moving towards practical applications. Future development directions include exploring the physical limits of light field manipulation, realizing the integration of multifunctional computational imaging and parallel image processing at the chip scale, and improving the efficiency and bandwidth of meta-devices. As shown in Figure 1, this paper outlines the core physical principles of meta-devices and reviews their applications in waveguides, lasers, spectrometers and sensors. Meanwhile, meta-optics technology is deeply integrating with cutting-edge fields such as 6G communication and quantum photonics; 6G components based on metasurface design have already achieved the core function of three-dimensional zoom [29]. And metasurface-assisted multimode quantum imaging technology also provides a new path for the practical application of quantum optics [30]; the application boundaries of metaphotonic devices are continuously expanding into interdisciplinary and high-value scenarios.

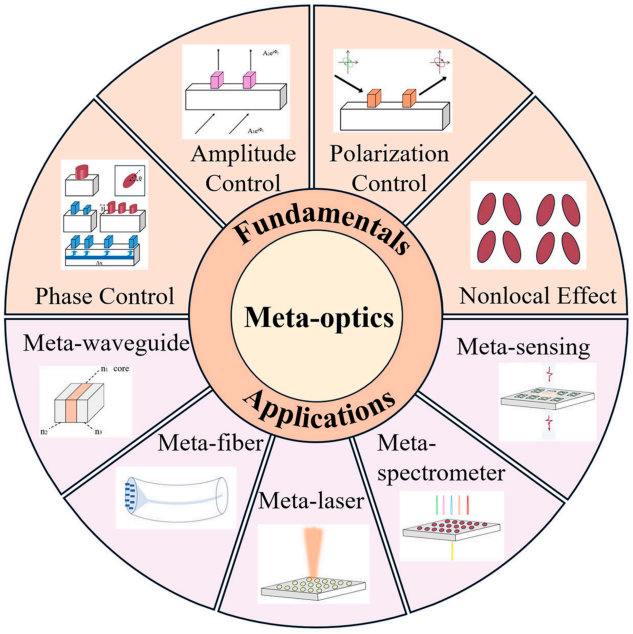


Figure 1. Fundamentals of meta-optics and applications.

2. Fundamentals

2.1. Phase Control

The core of meta-optics is the precise manipulation of the phase, amplitude, and polarization of a light field through subwavelength-scale arrays of meta-atoms. Phase manipulation is the fundamental basis for wavefront design in meta-optics. Optical metasurfaces achieve efficient and flexible manipulation of the beam wavefront by spatially encoding the phase response of meta-atoms at the subwavelength scale; this effectively suppresses higher-order diffraction, making the wavefront manipulation efficiency approach 1 [31]. In 2011, Capasso's team first introduced phase discontinuities using V-shaped nanoantennas, experimentally verifying the generalized laws of reflection and refraction of light, as shown in Figure 2a, thus laying the theoretical foundation for metasurface phase manipulation [32]. Based on geometric phase (Pancharatnam-Berry phase), a complete 2π phase coverage of circularly polarized light can be achieved by rotating the orientation angle (ϕ) of the anisotropic meta-atom from 0 to π. As shown in Figure 2b, by introducing geometric phase by adjusting its major axis orientation angle, phase delays are customized for left-handed and right-handed circularly polarized light respectively, realizing anisotropic modulation of spin angular momentum (SAM) [33].

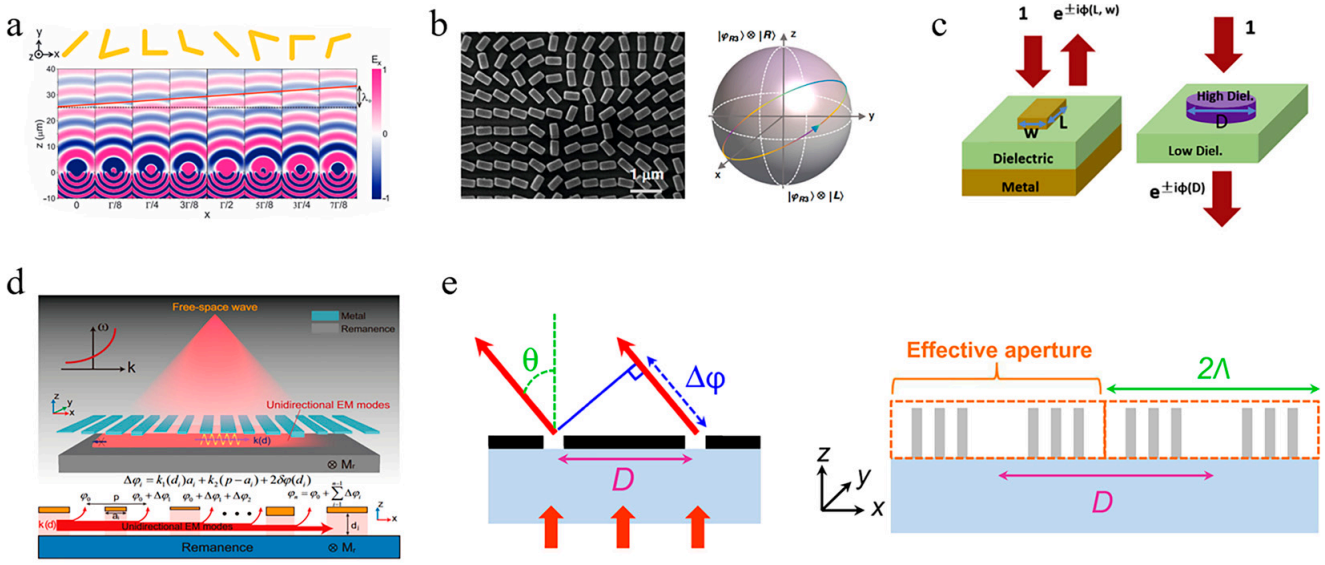


Figure 2. Phase control for metasurfaces. (**a**) Schematic diagram of metasurface phase gradient and generalized refraction based on a V-shaped antenna [32]. (**b**) SEM images of dielectric elliptical nanopillar meta-atomic arrays based on geometric phase [33]. (**c**) Schematic diagrams of two types of meta-atomic structures based on resonance phase [34]. (**d**) One-way waveguide-driven metasurface based on propagation phase [35]. (**e**) Broadband metasurfaces based on detour phase [36].

The optical response of anisotropic meta-atoms can be described by the Jones matrix, which is also the classic mathematical expression of metasurface phase modulation [34]. Its core form is as follows:

$$J(\varphi) = R(-\varphi) \cdot J_0 \cdot R(\varphi) \tag{1}$$

wherein, the intrinsic Jones matrix and the rotation matrix are respectively:

$$J_0 = \begin{pmatrix} t_x e^{i\varphi_x} & 0 \\ 0 & t_y e^{i\varphi_y} \end{pmatrix} \tag{2}$$

$$R(\varphi) = \begin{pmatrix} cos\varphi & -sin\varphi \\ sin\varphi & cos\varphi \end{pmatrix} \quad (3)$$

t_x and t_y are the transmission coefficients of the meta-atom to x-polarized and y-polarized light, respectively; φ_x and φ_y are the phase delays in the corresponding polarization directions; R is a two-dimensional rotation matrix, and φ is the spatial orientation angle of the meta-atom.

When circularly polarized light is incident, its polarization state can be expressed as follows:

$$\hat{e_{\pm}} = \frac{1}{\sqrt{2}}(\hat{e_x} \pm i\hat{e_y}) \quad (4)$$

where $\pm$ corresponds to right-handed/left-handed circular polarization, respectively. Combining Equation (1), the phase modulation expression of the transmitted light field under the circular polarization basis can be derived as follows [34]:

$$E_t^{\pm} = \frac{t_0 e^{i\varphi_0}}{2} cos\frac{\Delta\varphi}{2}\hat{e_{\pm}} + i\frac{t_0 e^{i\varphi_0}}{2} sin\frac{\Delta\varphi}{2} e^{\pm i2\varphi}\hat{e_{\mp}} \quad (5)$$

in the formula, $t_0 \approx t_x = t_y$ is the average transmission coefficient of the meta-atom, and the average phase delay and phase difference are respectively:

$$\varphi_0 = \frac{\varphi_x + \varphi_y}{2}, \Delta\varphi = \varphi_x - \varphi_y \quad (6)$$

Equation (6) clearly reveals the core principle of metasurface geometric phase manipulation: the transmitted light contains two components, co-polarized and cross-polarized, where the cross-polarized component carries a phase delay of $\pm 2\varphi$. This phase is uniquely determined by the orientation angle of the meta-atom, which is the geometric phase. When $\Delta\varphi = \pm\pi$, the meta-atom is equivalent to a half-wave plate, and the incident light can be completely converted into a cross-polarized component. At this time, by continuously rotating the orientation angle φ of the meta-atom within the range of 0 to π, continuous manipulation of the entire phase range of 2π can be achieved. This is also the most classic way to achieve metasurface phase manipulation [32,34].

By altering the geometric parameters of the meta-atom, its local resonance behavior and near-field mode distribution can be effectively controlled, thereby achieving precise encoding of the resonance phase. As shown in Figure 2c, this structure utilizes the F-P cavity effect to enhance the resonance response, and its phase delay characteristics are strongly correlated with its aspect ratio, providing a core phase encoding unit for reflective optical devices [34]. In propagation phase (dynamic phase) modulation, a square periodic array of high-refractive-index contrast medium nanopillars is designed. By combining the optical path length matching between the lattice period and the Mie resonance wavelength of the silicon nanopillar magnetic dipole, propagation phase delay modulation of light in a subwavelength structure is achieved. As shown in Figure 2d, this unidirectional waveguide-driven metasurface, with propagation phase modulation as its core design, independently modulates and extracts the phase and intensity of the wave through an imposed array of unit cells. It then constructs a preset target wavefront by progressively imposing the phase differences between adjacent unit cells, achieving arbitrary manipulation of the electromagnetic wavefront. Simultaneously, it breaks through the wavelength-scale modulation limitations of traditional metasurfaces, achieving highly efficient wavefront modulation at the deep subwavelength scale [35]. The detour phase achieves efficient directional output of specific diffraction orders by controlling the relative arrangement of meta-atoms and plasmonic resonance modes. As shown in Figure 2e, by optimizing the period and effective aperture of the metasurface array, the inherent wavelength dispersion

of the detour phase can be offset, achieving broadband and efficient phase modulation and polarization extinction in the 1100–1800 nm near-infrared band, providing a feasible path for multi-band optical devices [36]. Phase modulation technology is continuously evolving towards higher-order computation, intelligent design, and dynamic adjustability. Higher-order differentiators based on metasurfaces have already realized higher-order spatial mathematical operations on the optical field [37]; multilevel phase change material-based metalenses achieve dynamic phase control through phase transitions [38]; the introduction of the neighborhood attention Transformer algorithm further enables on-demand rapid design of metasurfaces [39]; meanwhile, the polarization dependence of wavefront spacing and Guo's phase in a strong focusing field also provides a new theoretical reference for high-precision phase control [40].

2.2. Amplitude Control

In high-performance applications such as holographic imaging and structured light field generation, optical devices require the simultaneous coordinated control of both the phase and amplitude of the optical field. Relying solely on phase control is insufficient to meet the demands of complex wavefront designs; therefore, amplitude control has become a crucial component of the principal system. The core of amplitude control lies in achieving spatial redistribution of incident light power through meta-atomic structure design. Currently, mainstream control strategies are all based on phase control, combined with reflection loss, polarization loss, and coherence loss to achieve controllable amplitude adjustment [41]. Amplitude modulation based on geometric phase is the most classic implementation method. As shown in the phase modulation formula above, the amplitude of the cross-polarization component of anisotropic meta-atoms is proportional to $\sin(\Delta\varphi/2)$. By controlling the intrinsic phase difference $\Delta\varphi$ of the meta-atoms, global modulation of the cross-polarization component amplitude can be achieved [42].

As shown in Figure 3a, Dorrah et al. [43] proposed a bilayer metasurface modulation scheme based on geometric phase. By stacking two layers of titanium dioxide (TiO_2) nanofins with different orientation angles, they achieved wavefront shaping and efficient amplitude distribution of linearly polarized light. This structure can complete wavefront shaping by relying solely on geometric phase, and the diffraction efficiency in the visible light band is as high as 80%. However, the bilayer alignment process is complex and the working bandwidth is limited. Figure 3b illustrates the principle of ultra-narrowband geometric phase metasurface modulation based on perturbed Mie resonators [44]. By introducing eccentric air holes into isotropic silicon nanodisks to construct the resonator array, global symmetry and pixel-level geometric phase modulation can be achieved, thereby exciting quasi-continuous domain-bound state resonance with high quality factors. This scheme can achieve a quality factor close to 3000 and diffraction-limited focusing at the resonance wavelength, but its amplitude response is highly dependent on the operating wavelength, which limits broadband applications [44].

As shown in Figure 3c, Xu et al. [45] revealed the mechanism for controlling the circular dichroism of chiral metamaterials through near-field coupling. By controlling the near-field coupling strength between adjacent chiral units, the absorption difference in left-handed and right-handed circularly polarized light can be significantly enhanced or suppressed while maintaining the chiral symmetry of the structure, thereby achieving passive control of the circular polarization amplitude. This method provides a new degree of freedom for the control of chiral optical fields, but the near-field coupling is extremely sensitive to the nano-gap, which increases the requirements for fabrication tolerance. Figure 3d shows a nonlinear polarization modulation scheme based on a single-crystal gold metasurface [46]. By utilizing the intrinsic anisotropy of gold crystals and designing

meta-atomic orientations to control the generation efficiency and polarization state of second harmonics, the amplitude and polarization of nonlinear optical signals can be controlled. This scheme extends amplitude modulation to the field of nonlinear optics, but the nonlinear conversion efficiency is generally low, requiring high-power pump light excitation.

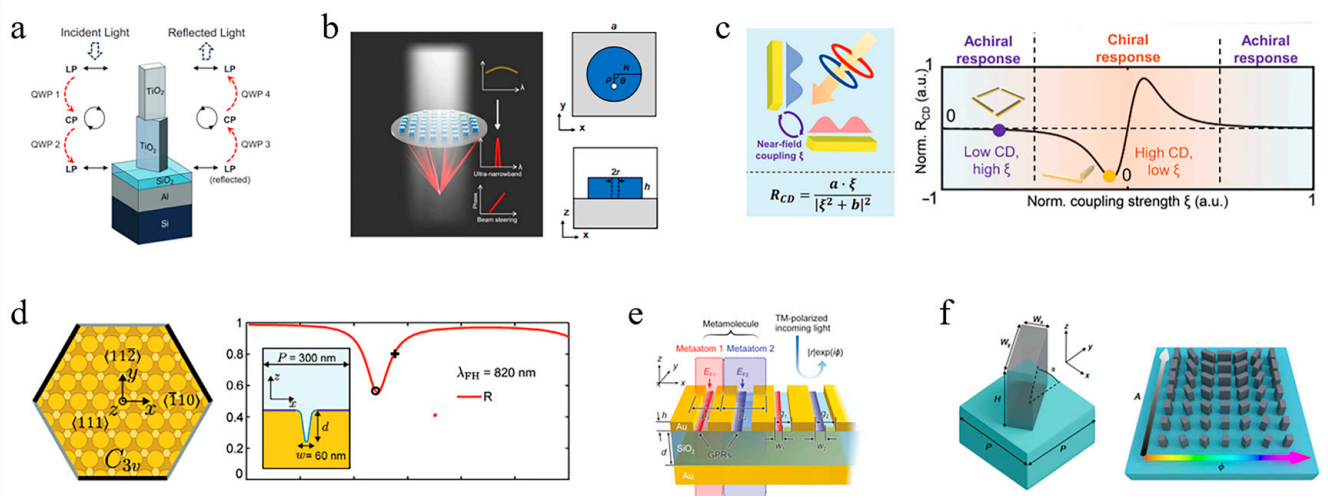


Figure 3. Amplitude control of metasurfaces. (**a**) Schematic diagram of a two-layer geometric phase metasurface structure [43]. (**b**) Ultra-narrowband geometric phase modulation using perturbation Mie resonators [44]. (**c**) Circular polarization dichroism altered by adjusting the spacing between adjacent units [45]. (**d**) Using crystal anisotropy to control the generation efficiency and polarization state of second harmonic waves [46]. (**e**) Dynamic independent control of transmission amplitude and phase is achieved by adjusting the Fermi level using the gate voltage [47]. (**f**) Completely independent control of the output light amplitude and phase can be achieved by simultaneously adjusting the size and orientation angle of the nanopillars [48].

The passive modulation schemes mentioned above are difficult to dynamically change after amplitude modulation, which limits their application in reconfigurable optoelectronic devices. As shown in Figure 3e, an active complex amplitude modulation scheme based on graphene plasmon supramolecular modulation was realized [47]. This work uses the gate voltage to modulate the Fermi level of graphene, thereby changing the resonance characteristics of the plasmon supramolecular modulation and realizing dynamic and independent control of the amplitude and phase of reflected light in the mid-infrared band [47]. This electronic control scheme provides an effective way for reconfigurable metasurfaces, but its modulation speed is limited by the RC constant of graphene, and the inherent ohmic loss of the plasmon structure will also reduce the modulation efficiency. Figure 3f shows the general scheme for independent amplitude and phase modulation based on all-dielectric metasurfaces proposed by the Overvig team [48]. This work achieves completely independent control of the output light amplitude from 0 to 1 and the phase from 0 to 2π at a single frequency by simultaneously changing the cross-sectional size of the dielectric nanopillar (modulating the propagation phase/birefringence) and the in-plane orientation angle (modulating the geometric phase). The scheme has a clear physical picture and simple design and has been successfully applied to high-fidelity two-dimensional and three-dimensional holographic imaging without iterative algorithms, providing a classic paradigm for multifunctional metasurfaces. However, once the passive structure is fabricated, its function is fixed and difficult to dynamically reconstruct. In order to overcome the limitations of passive modulation, the genetic optimization algorithm was applied to the design of metalenses to realize wavelength-dependent multifunctional amplitude-phase coordinated modulation [49]. Based on this control principle, a miniature tunable Airy

beam meta-device has also been successfully fabricated, providing a feasible solution for the miniaturization and tunability of structured light fields [50]. The fusion of amplitude modulation and holographic imaging is moving towards programmability. Novel devices based on programmable meta-holographic technology have achieved dynamic light field reconstruction, providing core technical support for scenarios such as reconfigurable holographic displays and optical encryption [51].

The above amplitude modulation schemes each have their own focus: bilayer geometric phase metasurfaces [43] are highly efficient but difficult to manufacture; perturbation Mie resonators [44] can achieve high Q narrowband response, but are highly sensitive to wavelength; chiral near-field coupling [45] can control circular dichroism, but has strict requirements for processing tolerance; single-crystal gold nonlinear metasurfaces [46] extend nonlinear control, but have low conversion efficiency; graphene active modulation [47] realizes electrically controlled dynamic amplitude modulation, but is limited by ohmic loss and modulation speed; the all-dielectric independent amplitude and phase modulation method [48] is simple to manufacture and covers the complete amplitude and phase range, but lacks dynamic reconstruction capability. The future direction is to combine phase change materials or MEMS technology to achieve high-efficiency dynamic amplitude modulation.

2.3. Polarization Control

Polarization is an important inherent property of light fields. Metasurfaces, with their unique optical response of anisotropic meta-atoms, can flexibly control the polarization of light fields and can be coordinated with phase and amplitude control, becoming the core support for multifunctional control of meta-optics [52]. Anisotropic subwavelength meta-atoms have significant differences in transmission/reflection coefficients and phase delays for orthogonally polarized light, which can be equivalent to subwavelength-scale optical waveplates [53]. Metasurfaces composed of them naturally possess polarization-related control characteristics, forming the physical basis for metasurface polarization control. Based on the theoretical framework of the Jones matrix, the phase distribution of wavefronts can be independently designed under any orthogonal polarization basis by coordinating the propagation phase and geometric phase of birefringent meta-atoms. As shown in Figure 4a, the longitudinal engineering metasurface developed by Tan et al. provides a new approach for three-dimensional vector holography [54]. This method controls the intensity and polarization state layer by layer along the optical axis, expanding the dimensional space of orthogonal polarization control. By optimizing the spatial layout of meta-atoms and introducing a polarization-dependent interference mechanism, Fan et al. established an independent control method for the complex amplitude of arbitrary orthogonal polarization states [55], as shown in Figure 4b. This scheme provides a general tool for vector light field generation. Jones matrix holography based on vector stacked diffraction and matrix polarity decomposition has been implemented in Figure 4c [56]. This technique achieves parallel polarization analysis through multi-channel wavefront control and exhibits programmable equivalent waveplate characteristics. Based on the mathematical framework of matrix optics [57], Figure 4d shows the design principle of using non-orthogonal polarization multiplexing to break through the information capacity limit [58]. This method extends the dimension of the Jones matrix to ten dimensions, effectively overcoming the channel constraints of traditional orthogonal multiplexing schemes. The polarization regulation device integration and practical application of polarization modulation have become an important development direction. The inverse design of Jones matrix metasurfaces provides a core method for the fabrication of high-performance metapolarizers [59]. Miniaturized snapshot polarization stereo imaging devices based on

polarization modulation [60] and photon spin-dependent double Bessel beam generation devices [61] have also been successfully demonstrated. The large-scale application of polarization modulation is inseparable from low-cost batch fabrication processes. Chiral imaging metasurfaces based on nanoimprint technology have achieved centimeter-scale large-area fabrication, providing an integrated solution of process and function for the industrial application of polarization modulation [62]. In addition, dielectric metasurfaces can also achieve simultaneous detection of transverse and longitudinal displacements through polarization modulation, providing a new path for high-precision sensing [63].

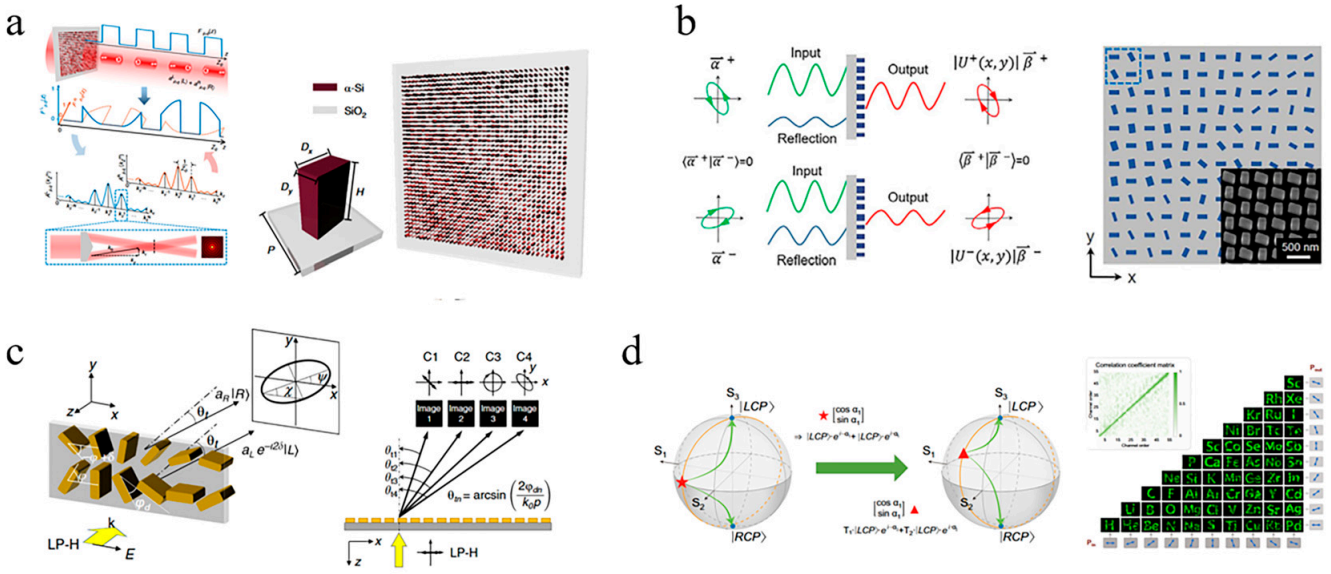


Figure 4. Polarization control using shaped birefringent metasurfaces. (**a**) Achieving three-dimensional vector holography through longitudinally engineered metasurfaces [54]. (**b**) Completely and independently controlling the complex amplitude of arbitrary orthogonal polarization states [55]. (**c**) Jones matrix holography using birefringent metasurfaces [56] (**d**) Breaking through the holographic information capacity using non-orthogonal polarization multiplexing [58].

2.4. Nonlocal Effect

Nonlocal effects break through the traditional local optics control paradigm. Under the local response mechanism, the optical behavior of a device at a certain spatial location is determined only by the incident light field at that location; that is, the output response of each point on the metasurface is independent and does not interfere with each other. However, the response described by nonlocal optics depends on the distribution of the incident light field in the extended spatial region [64], enabling the device to respond to the global characteristics of the incident wavefront, thereby realizing functions that are difficult to achieve by local devices, such as spatial frequency filtering and edge detection.

In periodic optical systems, continuous domain bound states are a typical physical mechanism for realizing nonlocal responses [65]. Although these modes are in the continuous radiation domain, they are perfectly localized due to symmetry constraints or interference cancellation, theoretically possessing an infinite quality factor and being completely decoupled from the far field [66]. In practical applications, structural perturbations are mainly introduced to excite continuous domain quasi-bound states, achieving weak coupling with the far field while maintaining the high-quality factor. As shown in Figure 5a, by adjusting the structural asymmetry parameters, resonances with extremely high-quality factors can be excited at a specific frequency, and their electric fields are strongly localized within the dielectric layer [67]. Wavefront modulation based on nonlocal resonant modes provides a new approach for the design of multifunctional devices. Figure 5b shows the

chiral selective anomalous deflection achieved by using a guided-mode resonant metasurface [68]. By designing a nonlocal metasurface with symmetry, the circularly polarized incident light can obtain a higher-order geometric phase related to the rotation angle during the cross-polarization conversion process, thereby realizing wavefront modulation based on the chirality of the incident light. In addition, the topological properties of the continuous domain-bound state open up new avenues for chiral optical modulation. As shown in Figure 5c, by breaking the structural symmetry, the polarization singularity can be split from the linear polarization point into the circular polarization point, thereby realizing a quasi-continuous domain-bound state mode with circular polarization selectivity [69]. This resonant chiral effect based on the continuous domain bound state provides a new platform for nonlinear harmonic generation and chiral optical field modulation. Quasi-continuous domain bound states (quasi-BIC) have become the core direction for the practical application of nonlocal effects. Based on quasi-BIC, dual-wavelength chiral metasurfaces [70] and switchable optical field manipulators [71] have realized the flexible switching between chiral modulation and optical field manipulation. At the same time, the synthesis of configurable topological photonic polycrystalline technology with mixed dimensions has also provided a new structural design idea for the integration of nonlocal effects and topological photonics [72].

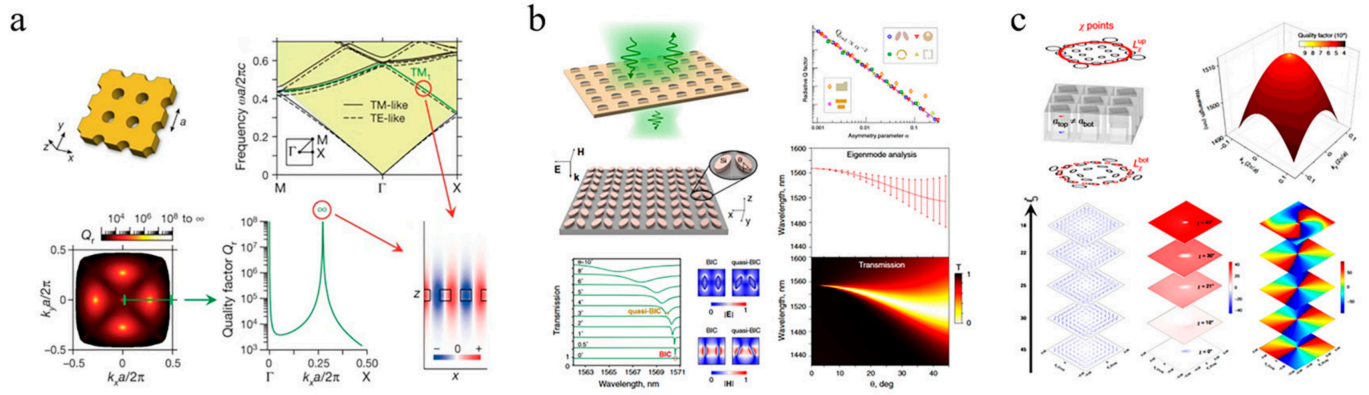


Figure 5. Classification of BICs. (**a**) Random continuous-domain bound state [67]. (**b**) Quasi-continuous-domain bound state. Chiral selective anomalous deflection of circularly polarized light is achieved by relying on high-Q quasi-continuous-domain bound states [68]. (**c**) Chiral continuous-domain bound state. By breaking the symmetry through structural perturbation, the polarization singularity is induced to split from the linear polarization point into the circular polarization point, thereby exciting a chiral BIC mode with precise circular polarization selectivity [69].

It should be noted that although BIC and q-BIC can achieve extremely high quality factors, their resonance characteristics are very sensitive to the incident angle: when the incident wave vector deviates from the Γ point, radiation loss increases sharply, and the Q value drops rapidly. Furthermore, q-BIC relies on minute breaks in structural symmetry to modulate radiation loss; any manufacturing error (such as nanopore misalignment or dimensional deviation) will lead to unexpected changes in symmetry, resulting in an actual Q value far lower than the theoretical design value. Therefore, in practical devices, tolerance analysis and advanced processes need to be combined to balance Q value and manufacturing yield. To improve the quality factor of BIC-based devices, various strategies can be adopted, including optimizing structural parameters (such as nanopore size and period) to make the quasi-BIC mode closer to the ideal BIC, thereby reducing radiation loss; introducing multilayer or composite dielectric structures to enhance optical field localization; and using high-precision manufacturing processes such as electron beam lithography and atomic layer deposition to reduce symmetry breaking. Recent studies have

shown that extremely high Q values can be achieved in specific wave vector directions by designing symmetric protected BICs or accidental BICs [73]. Furthermore, by combining topology optimization and reverse design methods, the Q factor can be maximized with limited manufacturing tolerances [74].

3. Meta-Waveguides

Traditional waveguides are the core basic components of integrated photonic circuits (IPCs). Their optical field manipulation capability mainly relies on the total internal reflection effect of light and the macroscopic geometry of the waveguide, resulting in limited functionality and control flexibility. The rise in metamaterials and metasurfaces has provided a new paradigm for the flexible manipulation of subwavelength electromagnetic waves, breaking through the traditional optical framework [75,76]. Based on this, researchers have combined subwavelength meta-atoms with traditional waveguide structures, proposing the emerging research direction of "meta-waveguides" [77]. The versatility of these devices relies primarily on phase control, and some schemes also introduce nonlocal effects to achieve narrowband extraction and color routing. The core feature of meta-waveguides is that they utilize artificial equivalent parameters (such as equivalent wave vector and equivalent refractive index) introduced by subwavelength unit structures (meta-atoms) to break through the control limits of traditional waveguides and achieve more compact and multifunctional optical field manipulation.

Planar meta-waveguides, based on integrated photonic chip technology, combine subwavelength metastructures with planar waveguides. This overcomes the limitations of traditional waveguides that rely solely on total internal reflection and macroscopic geometry for optical field manipulation. They exhibit significant advantages in dispersion engineering, mode manipulation, functional integration, and on-chip system adaptation, becoming a research hotspot in integrated photonics.

All-dielectric meta-waveguides provide a novel pathway for high-density on-chip functional integration. The all-dielectric Huygens meta-waveguide proposed by Sırmacı et al. [78] (Figure 6a) further optimizes the waveguide transmission performance. This waveguide provides resonant energy by means of electromagnetic dipole Mie-type resonance with spectral overlap, achieving a propagation loss as low as 0.4 $dB \cdot mm^{-1}$ in the telecommunication spectrum range, which is an order of magnitude higher than the performance of existing Mie resonant waveguides. It also supports negative group refractive index and anomalous dispersion in the 60 nm spectrum range and can realize a resonant-protected compact waveguide bending structure and efficient beam splitting within a compact propagation length of 320 nm, providing new possibilities for enhancing light-matter interaction and developing on-chip quantum and nonlinear optical devices. Cui et al. [79] proposed and experimentally verified a dynamic switching method from coherent perfect absorption (CPA) to parametric amplification (PA) based on a nonlinear artificial surface plasmon waveguide. As shown in Figure 6b, this study is based on a carefully designed nonlinear artificial surface plasmonic waveguide structure. By dynamically adjusting the phase relationship between the input pump wave and the signal wave, the output power of the signal wave can be flexibly and continuously modulated, providing a new path for the active control of electromagnetic signals [79].

The dielectric silicon-based phase gradient meta-waveguide designed by Wang et al. [80] breaks through the design limitations of traditional on-chip reflectors. As shown in Figure 6c, by introducing phase gradient meta-units on the sidewalls or top of the waveguide, precise control of the propagation direction is achieved. The fabricated meta-waveguide reflector achieves high-fidelity reflection of the TE_{00} mode in a broadband range of greater than 200 nm, with a reflectivity of up to 97%. Based on this, the Fano resonator,

FP resonator, multimode switch and other devices further developed can achieve high-quality factor resonance and multimode modulation by relying on the mode interference effect and have a strong tolerance for manufacturing errors. They can be used as standard components of integrated photonic chips in the field of on-chip optical information processing and sensing [80]. In addition to the phase gradient meta-waveguide based on regular meta-atomic arrays, the inverse design method provides a free design space for the functional integration of planar meta-waveguides. Chen et al. [81] designed a freeform metasurface coupler on a Si_3N_4 waveguide based on the adjoint topology optimization method, achieving directional coupling from arbitrary incident polarization states to arbitrary TM modes (including higher-order modes such as TM_{01} and TM_{10}). The target polarization mode purity exceeded 90%, and the coupling efficiency reached a maximum of 43%. Furthermore, through multi-objective optimization, the device achieved coupling of orthogonally incident polarizations (E_x and E_y) to TM_{01} and TM_{10} modes respectively, on the same waveguide, and utilized mode position to generate mixed modes with controllable incident polarization and on-chip orbital angular momentum (OAM) beams. This work demonstrates the powerful capabilities of inverse design methods in meta-waveguides, providing a new path for on-chip polarization diversity, mode multiplexing, and vortex source integration [81].

Faced with the application requirements of planar meta-waveguides in high-capacity optical field manipulation and multi-dimensional multiplexing, the synergistic modulation of multi-phase mechanisms has become an important research direction for breaking through traditional modulation methods. Li et al. [82] proposed a meta-atoms design method that integrates detour phase and geometric phase, as shown in Figure 6d. They realized the full parametric modulation of the Jones matrix and demonstrated four independent amplitude and phase channels through a single on-chip metasurface experiment. The team further introduced propagation phase modulation and achieved the decoupling of the Jones matrix between the forward and backward propagation guided waves through the coordinated modulation of detour phase, geometric phase and propagation phase, thereby achieving the directional multiplexing of guided wave radiation [82]. This research provides a new design idea for high-capacity multiplexing of guided wave radiation and effectively expands the application boundaries of planar meta-structure waveguides in optical communication, optical display and augmented/virtual reality fields.

Li and Song et al. collaborated to realize an on-chip topological metasurface in an all-dielectric architecture (Figure 6e). By screening the geometry of Si meta-atoms on the Si_3N_4 waveguide on a large scale, they achieved a 2π topological phase shift around the exception point. Combined with the Pancharatnam-Berry phase decoupling orthogonal circular polarization channels, they realized the independent coding degree of freedom control of holographic generation and realized floating holographic visualization in real scenes [83]. This all-dielectric on-chip solution eliminates ohmic loss and can be integrated with other on-chip meta-devices, effectively solving the performance shortcomings of the first-generation AR on-chip integrated system. It has important application prospects in the fields of next-generation AR devices, multiplexed information storage, and advanced optical display [83]. Furthermore, Li et al. [84] proposed and experimentally verified an on-chip metasurface color router based on symmetry-broken quasi-continuous domain bound states (q-BICs). The study achieved the extraction intensity modulation and narrowband spectrum extraction of coupled light waves by precisely controlling the scale and asymmetry of meta-biatomic pairs. Through spatial mapping and q-BIC-assisted pixel cascading, an on-chip multiplexed color router was fabricated, which can selectively route the main wavelength to free space from different spatial positions of the waveguide. As shown in Figure 6f, this device, based on an on-chip light propagation scheme, significantly improves

energy utilization efficiency (EUE) compared to traditional designs while achieving spatial multiplexing. This device has the potential for miniaturization and integration and is expected to open up new paths for multiplexed information routing, intelligent integrated photonic systems, and next-generation wearable display technologies [84]. The application of planar meta-waveguides has been extended to the field of 6G communication. 6G components based on planar meta-waveguides have realized a three-dimensional zoom function, providing core device support for 3D optical field control of 6G communication [29].

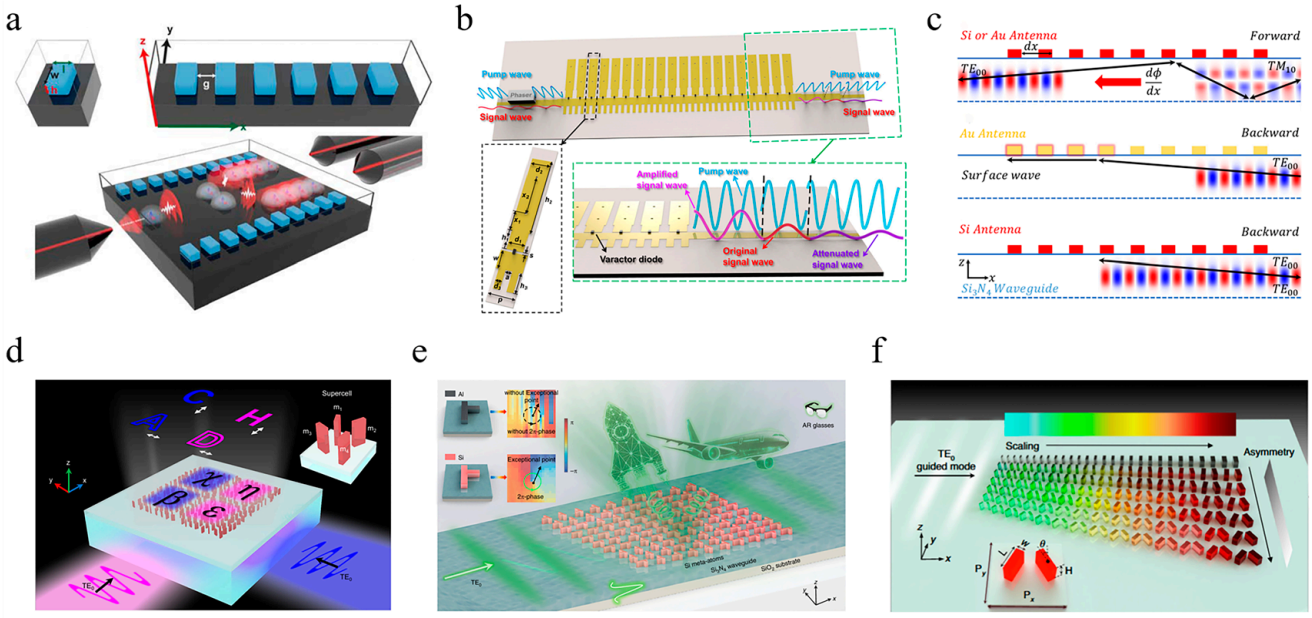


Figure 6. Meta-waveguides. (**a**) Schematic diagram of a Huygens superstructure waveguide [78]. (**b**) Nonlinear artificial surface plasmon polariton waveguide [79]. (**c**) Schematic diagram of a phase gradient metastructure waveguide, where the unidirectional phase gradient $\frac{d\varphi}{dx}$ can be introduced by an all-dielectric Si or a metallic Au [80]. (**d**) Conceptual illustration of guided wave radiation through an on-chip metasurface composed of four-element unit cells [82]. (**e**) Schematic diagram of an on-chip all-dielectric metasurface based on topological phase coding for dual-channel holographic display [83]. (**f**) Schematic diagram of an on-chip color routing metasurface based on q-BICs inspired by physics [84].

For several representative works in the field of meta-waveguides, we classify and compare them according to their physical mechanisms and functional goals, mainly covering four aspects: dispersion and loss control, mode manipulation and reflection, multi-phase co-coding, and nonlocal color routing. In terms of dispersion and loss control, Huygens meta-waveguides [78] have the advantages of extremely low propagation loss and anomalous dispersion, making them suitable for on-chip quantum optics, but they lack active tuning capability, while nonlinear artificial surface plasmon waveguides [79] achieve dynamic tunability but are limited by ohmic loss and narrowband operation. In terms of mode manipulation and reflection, phase gradient waveguides [80] provide a trade-off between broadband high reflectivity and sensitivity to manufacturing errors; reverse-designed couplers [81] pursue a balance between design freedom and computational cost. In terms of multi-phase co-coding, off-axis/geometric phase co-coding schemes [82] achieve multi-channel independent modulation, while topological metasurfaces [83] exchange manufacturing precision for dual-channel holographic functionality. In terms of non-local color routing, the q-BIC scheme [84] presents a clear trade-off between energy efficiency and operating bandwidth and symmetry tolerance.

The integration of metasurfaces with planar waveguides represents a transformative development in the field of integrated optics. By deeply fusing the powerful free-space light-field manipulation capabilities of metasurfaces with the on-chip light transmission and processing capabilities of planar waveguides at the chip scale, this approach overcomes the performance and functional bottlenecks inherent in traditional photonic devices [85].

4. Meta-Fibers

Since the advent of optical fiber in the 1960s, it has become the core carrier in fields such as optical communication, fiber optic sensing, and laser processing [86–88]. The accuracy of phase modulation is a key factor restricting the performance of optical functional devices. Meta-fibers integrate subwavelength meta-atoms on the fiber end face or core, combining the low-loss transmission advantage of optical fiber with the precise modulation capability of metasurfaces, and have become an important branch of meta-waveguides [89,90]. Recent studies have demonstrated the integration of metasurfaces on the fiber end face to achieve functions such as mode separation, promoting the functional diversification of meta-fibers [91].

The core modulation mechanism of meta-fibers originates from the equivalent medium effect of subwavelength meta-arrays: when the period P of meta-atoms (such as silicon-based or silicon dioxide-based nanopillars) is much smaller than the working wavelength λ ($P \ll \lambda$), the array can be equivalent to a homogeneous medium; if the meta-atoms have geometric anisotropy (such as elliptical cylinders or rectangular nanopillars), the equivalent medium exhibits anisotropy, providing support for polarization-sensitive designs [92]. At this time, the phase delay (φ) generated by the propagation of light waves in the core of the meta-fiber satisfies:

$$\varphi = \frac{2\pi}{\lambda} n_{\text{eff}} H \tag{7}$$

H represents the thickness/length of the core meta-region. By precisely controlling the geometric parameters of the meta-atoms (such as diameter, side length, aspect ratio, and spatial arrangement), the equivalent refractive index n_{eff} can be continuously adjusted. Combined with the gradient design of the core meta-region, full phase coverage from 0 to 2π can be achieved [93]. This mechanism is the core of wavefront modulation in meta-fibers. Compared with traditional gradient refractive index fibers, it has higher phase modulation accuracy and more flexible functional integration. From a more fundamental perspective, this ability to cut electromagnetic waves from one dimension to multiple dimensions is the core advantage of metaphotonics [41].

Mie resonance provides a theoretical basis for the design of dielectric meta-atoms. By exciting the electromagnetic dipole mode in subwavelength high refractive index particles, significant local field enhancement and resonant phase dispersion can be achieved in specific wavelength bands, thus laying a physical foundation for constructing fiber functional layers with specific equivalent parameters [94]. Dielectric metasurfaces based on Mie resonance provide an effective way to realize wavefront manipulation of fiber integration. By precisely designing the geometric parameters of units such as silicon nanopillars, efficient transmission phase modulation can be achieved in a wide band, providing a feasible technical solution for the development of fiber end-face beam shaping devices [95]. The transition from passive metamechanical modulation to active emission is a key direction for the functional expansion of fiber metamaterials. By utilizing the high-quality factor leakage resonance formed by the continuous domain bound states in the semiconductor nanoantenna array, low-threshold, tunable wavelength and direction laser emission can be achieved, opening up a new research path for the development of novel meta-fiber lasers [96].

In other words, meta-fibers mainly rely on phase control and polarization control. The former achieves wavefront shaping through equivalent refractive index adjustment, while the latter achieves polarization-sensitive response through anisotropic structures. Some devices also introduce Mie resonance to enhance the local optical field.

Xu and Wang et al. [97] proposed a mode-preserving separation device (FIMMERS) based on fiber-integrated metasurfaces. As shown in Figure 7a, this device uses a mode space symmetry partitioning optimization strategy to achieve efficient separation of three overlapping modes, LP_{01}, $LP_{11}a$, and $LP_{11}b$, and can maintain a mode fidelity of up to 92% in the entire C-band without the need for a mode conversion step. The device size is only about 600 μm, which is nearly two orders of magnitude smaller than that of traditional mode division multiplexing devices [97]. Based on this separator, the team further realized the encrypted transmission of full-color images using a mode combination as the key, significantly improving information security. This work provides key technical support for highly integrated mode division multiplexing systems. Meanwhile, remote focusing control has become another important direction for the functional expansion of meta-fibers. Markus A. Schmidt et al. [98] achieved precise focusing control of light coupled to different fiber cores by 3D nanoprinting phase holograms on the end face of a 37-core single-mode fiber, as shown in Figure 7b. The focal position can be remotely adjusted without crosstalk, and the experiment and design are highly consistent. Based on this, Sun et al. [99] further proposed a monolithic integration scheme of dual-core fiber and 3D nanoprinted phase holograms, as shown in Figure 7c. By adjusting the relative power of the modes to generate controllable interference patterns, dynamic spatial focusing without alignment is achieved, with a total focal offset exceeding 3 μm, and the advantages of fast modulation speed and strong temperature stability are also present. These studies demonstrate the flexibility and reliability of all-fiber integrated dynamic focusing systems.

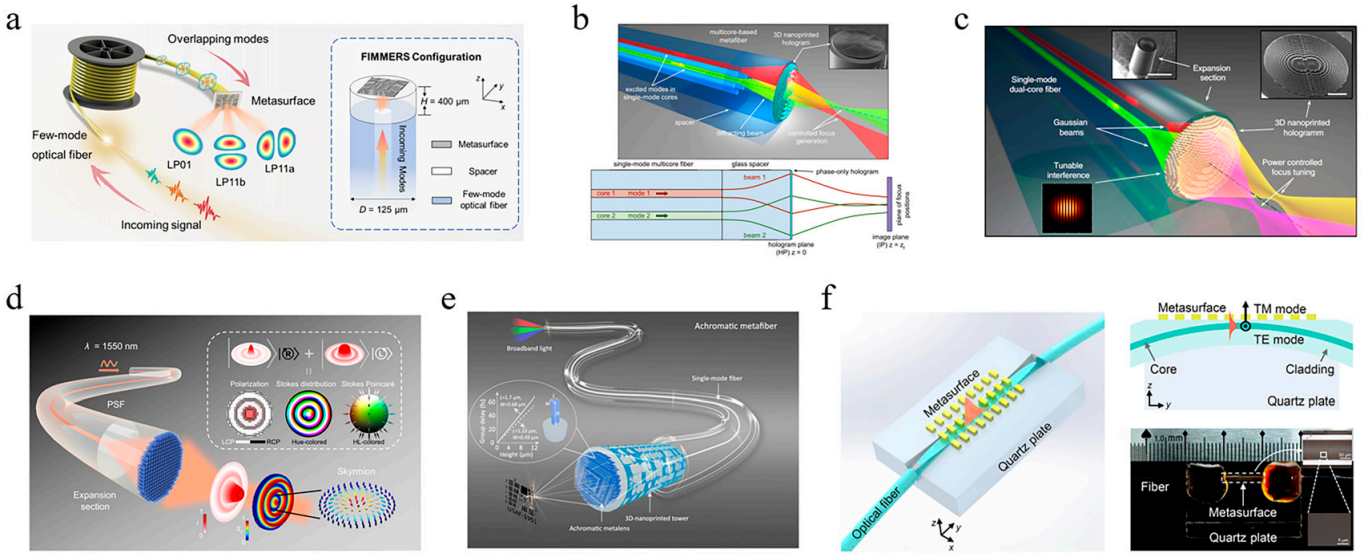


Figure 7. Meta-fibers. (**a**) Schematic diagram of FIMMERS, illustrating how an input signal with overlapping modes via FMF can be split into LP_{01}, $LP_{11}a$, and $LP_{11}b$ by a metasurface integrated on the end face [97]. (**b**) Adjustable focusing operation of a pure phase hologram using a multi-core fiber interface [98]. (**c**) Working principle of a synergistic meta-fiber [99]. (**d**) Schematic diagram of skyrmion excitation from a meta-fiber [100]. (**e**) Principle of achromatic meta-fiber for achromatic focusing and imaging [101]. (**f**) Conceptual diagram and optical image of a planar sidewall integrated meta-fiber [102].

Xiao and Shen et al. [100] used "fiber lab" technology to design and experimentally verify skyrmion emitters with various topologies (Figure 7d), achieving robust transmission

of subwavelength Stokes skyrmions for the first time, providing an effective solution for on-chip integration of topological beams. This research opened up a new path for the integration of topological photonics and fiber optic communication and also laid the foundation for the application of topological structures in information encoding and transmission.

In broadband imaging applications, Ren et al. integrated 3D achromatic diffraction metalenses on the end face of a single-mode fiber using 3D laser nanoprinting technology, constructing an achromatic meta-fiber (Figure 7e) [101]. Utilizing the height degree of freedom of the nanopillars, a wide group delay modulation range of 8 to 14 fs was achieved, with a time-bandwidth product of 21.34. The device achieves polarization-insensitive diffraction-limited focusing across the entire telecommunications band from 1.25 to 1.65 μm. When applied to fiber confocal scanning imaging, it achieves a spatial resolution of 4.92 μm, with significantly better imaging clarity than traditional chromatic aberration meta-fibers. This provides key technical support for hyperspectral endoscopic imaging and deep tissue imaging. Sun and Mao et al. [102] proposed a new paradigm of planarized sidewall integration (Figure 7f). Through fiber-substrate planarization, a large-area metasurface is constructed in situ on the side-polished fiber (SPF). The coupling effect of the evanescent field is amplified by long-range resonant near-field coupling, which significantly enhances the linear and nonlinear optical responses. The gold nanorod-based meta-fiber saturable absorber device they developed has achieved ultra-low threshold all-fiber ultrafast laser output, providing a multifunctional fiber laboratory platform for enhancing linear and nonlinear optics.

Unlike planar waveguides, various meta-fiber schemes differ significantly in integration location and control objectives and can be summarized into five categories: mode separation and encrypted transmission, remote focusing control, topological beam excitation, achromatic imaging, and side-integrated nonlinear modulation. Mode-preserving splitters [97] have advantages in small size and high fidelity but require precise alignment; 3D nanoprinting schemes [98,99] achieve remote crosstalk-free focusing but are limited by manufacturing resolution; achromatic metasurface fibers [101] expand the working bandwidth, but the processing difficulty increases accordingly; side-integrated schemes [102] enhance the nonlinear response, while end-face integrated structures are simple but have limited functionality. Topological beam excitation [100] represents a cross-exploration towards topological photonics.

The integration of metasurfaces with optical fibers effectively resolves critical bottlenecks in optical fiber systems regarding miniaturization, functional integration, and the precise manipulation of complex light fields at the fiber end-face, which brings new opportunities for next-generation high-sensitivity sensing, singularity lasers, and topological bandgap manipulation [103–105]. The integration of meta-fibers and topological photonics continues to deepen, and robust transmission of spin Stokes skyrmions has been achieved based on meta-fibers [106].

5. Meta-Lasers

In 2015, Xu et al. first demonstrated a terahertz vertical external cavity surface-emitting laser (THz VECSEL) based on an amplified reflective array metasurface, showcasing core technological advantages that traditional lasers cannot match [107] and formally opening up a new research direction for multidimensional precise control of metasurface lasers [108]. Unlike traditional lasers that rely on resonant cavity mode selection, meta-lasers mainly rely on phase control, polarization control, and nonlocal effects to achieve arbitrary wavefront shaping, chiral light field emission, and low-threshold high-coherence oscillation, respectively.

Song and Xiao et al. [109] proposed and realized a new type of laser with arbitrarily tunable wavefronts (Figure 8a), breaking through the limitations of traditional lasers in terms of mode shape, polarization state, and angular momentum. This work enabled the free customization of the laser emission wavefront, providing a new approach for the application of lasers in precision measurement, optical communication, and high-resolution imaging. Regarding organic lasers, Daegwang Choi et al. [110] used small molecular ion-isolated lattices (SMILES) as the active medium, combined with PMMA as a resist, and directly patterned them using electron beam lithography to construct a metasurface structure without etching, as shown in Figure 8b. This structure supports photonic BIC with Γ-point symmetry protection, achieving highly coherent organic laser emission and demonstrating the potential of metasurfaces in simplifying fabrication processes and improving laser performance. Zheng, Kivshar, Peng, et al. [111] focused on the generation and manipulation of chiral light fields. They designed and fabricated a twisted bilayer structure composed of two semiconductor metasurfaces, as shown in Figure 8c, and utilized its inherent structural chirality to achieve orbital chiral laser emission. This laser can operate in a single mode over a wide spectral range of 250 nm, and its chiral orbital characteristics originate from the non-Hermitian coupling between waveguide resonant modes. This research lays the foundation for the application of chiral light sources in fields such as biological detection, optical manipulation, and communication.

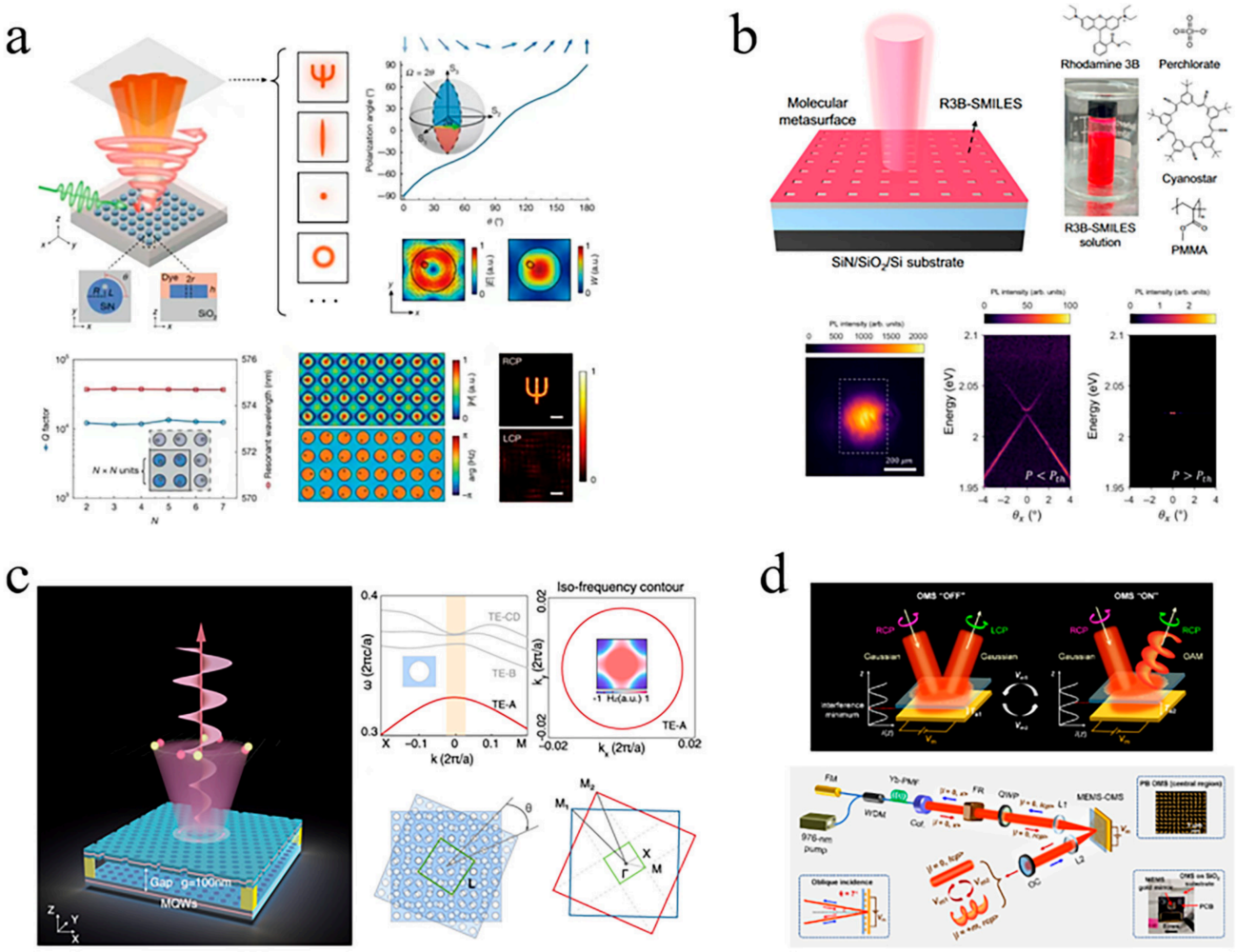


Figure 8. Meta-lasers. (**a**) Metasurface laser concept [109]. (**b**) BIC laser emission in etch-free molecular metasurfaces [110]. (**c**) Structures for intrinsically orbital chiral lasers [111]. (**d**) Mode-switchable vortex laser design [112].

Regarding the speed and high purity of dynamic control, Wang et al. [112] demonstrated a vortex fiber laser based on an electrically driven MEMS optical metasurface (MEMS-OMS) (Figure 8d). This device can achieve fast and high-contrast switching between Gaussian mode and multiple vortex modes at a wavelength of about 1030 nm, with a mode purity of over 95% and a response time of about 100 microseconds. This device combines MEMS technology with metasurface control, providing a new solution for achieving high-purity and fast-switching laser modes, and is suitable for optical tweezers, optical processing and intelligent photonics systems. Metasurface lasers are developing towards ultrafast and intelligent directions, and ultrafast nanophotonics technology provides core theoretical and technical support for the ultrafast modulation of metasurface lasers [113]. In addition to wavefront and mode control of single lasers, metasurface lasers are expanding from single devices to coupled arrays and novel physical effects. Tang et al. [114] realized long-range tunable coupling (up to tens of micrometers) between microlasers based on BIC metasurfaces and demonstrated dynamic switching of non-Hermitian zero-mode lasers by adjusting pump intensity and delay.

The meta-lasers can be classified according to their control mechanisms into highly coherent organic BIC lasers, chiral-controlled bilayer lasers, rapidly dynamically switching MEMS vortex lasers, and long-range coupled BIC laser arrays. Organic BIC lasers [110] are characterized by low threshold and high coherence, but they have strict requirements for structural symmetry; chiral bilayer lasers [111] achieve broadband single-mode chiral emission, but at the cost of complex manufacturing processes; MEMS vortex lasers [112] provide rapid switching at the microsecond level and high mode purity, but are limited by the fatigue life of MEMS structures; long-range coupled BIC laser arrays [114] demonstrate the dynamic switching of non-Hermitian zero modes, providing a new idea for the coordinated control of laser arrays, but their coupling distance and pumping conditions still need to be finely optimized.

6. Meta-Spectrometers

Spectrometers, which are used to measure the distribution of light intensity as a function of wavelength, serve as a core tool for analysis. Traditional spectrometers are primarily based on dispersion or interference principles. However, it suffers from drawbacks such as large size and structural complexity, which limit its application in portable scenarios. Meta-spectrometers overcome this limitation, and their wavelength resolution can be achieved based on different physical mechanisms such as phase control, amplitude control, and polarization control. Among these, nonlocal effects can further improve the spectral resolution of the resonance scheme. With advancements in nanofabrication techniques, meta-spectrometers can effectively address these issues and are gradually emerging as a vital method for the detection of optical characteristics [115–121]. Altug et al. developed "Imaging-based molecular barcoding with pixelated dielectric metasurfaces" for the chemical identification and compositional analysis of substances (Figure 9a). Each resonance within the two-dimensional dielectric metasurface material is tuned to a discrete frequency, enabling molecular absorption features to be read out at multiple spectral points [122]. Y. Yang et al. propose and experimentally demonstrate a single-shot spectroscopic ellipsometry system using a passive silicon-based metasurface array for spectro-polarimetric encoding in the visible frequency regime, with the system schematically depicted in Figure 9b [123]. Z. Yang et al. proposed a miniature spectrometer based on metasurfaces. This device leverages the optical properties of q-BIC by tuning the geometric parameters of the meta-array, as shown in Figure 9c, enabling the flexible adjustment or expansion of the operating band [124]. Moreover, Jang et al. report the use of double-layer disordered metasurfaces as a spatio-spectral mixer (Figure 9d), providing a versatile

complex mapping characteristic of high spectral sensitivity within a small footprint of 1 cm [125].

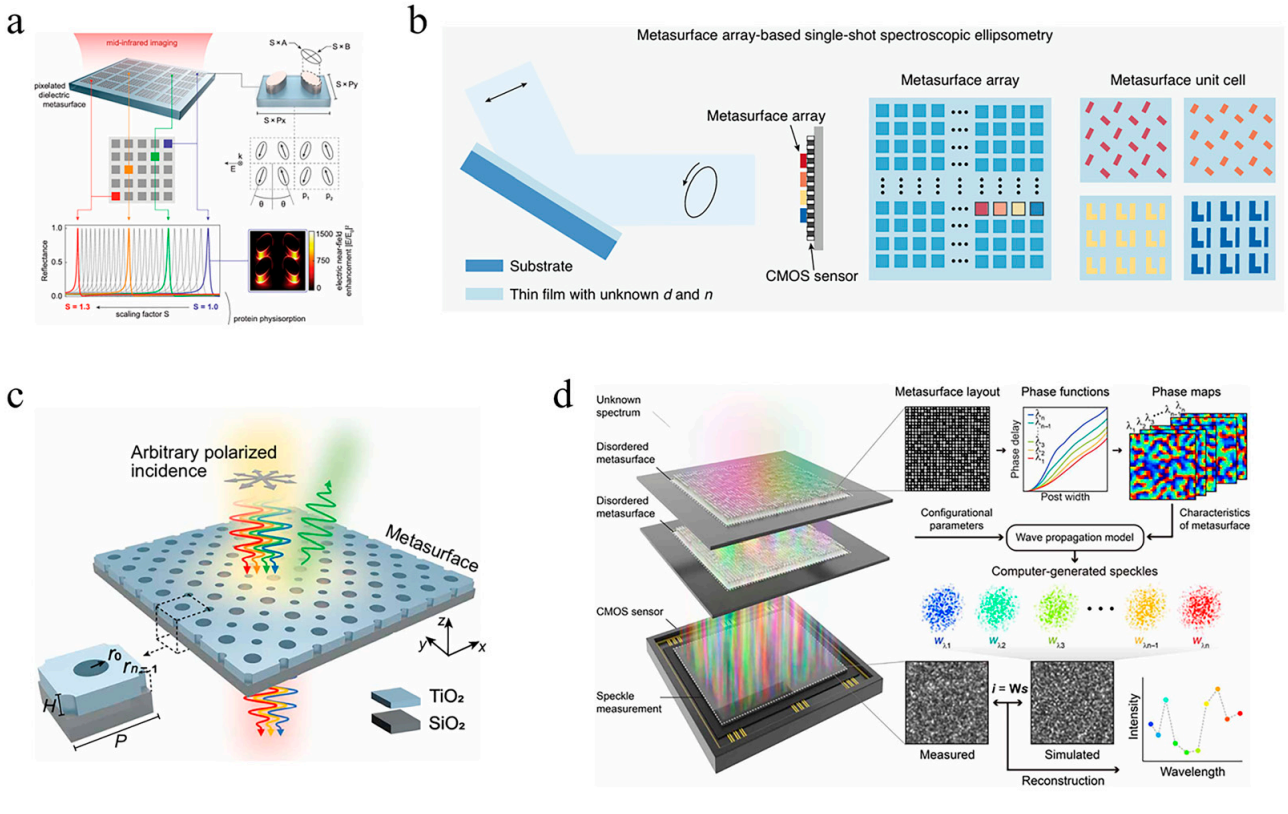


Figure 9. Meta-spectrometers. (**a**) Molecular fingerprint detection based on pixelated dielectric metasurfaces [122]. (**b**) Schematic diagram of a single-shot spectral ellipsometry measurement system based on metasurface arrays [123]. (**c**) Pixelated metasurfaces with polarization-independent q-BICs [124]. (**d**) Schematic diagram of a reconstructive spectrometer based on bilayer disordered metasurfaces [125].

Consequently, meta-spectrometers leverage the powerful light-field manipulation capabilities of subwavelength structures. By achieving breakthroughs in both performance and size, they effectively address the limitations of traditional spectrometers, demonstrating great performance and design flexibility in the realms of miniaturization, on-chip integration, and computational spectral reconstruction.

The implementation paths of meta-spectrometers can be divided into two categories: resonance type and scattering type. Resonance-type schemes [122,124] utilize high-quality-factor resonance to achieve narrowband high-sensitivity detection, but the working band is limited and sensitive to angle; scattering-type schemes [125] obtain broadband response and high spectral sensitivity through spatial-spectral hybrid encoding, but at the cost of spectral resolution. In addition, single-spectral ellipsometry systems based on metasurface arrays [123] integrate polarization modulation and wavelength encoding, expanding the functional dimensions, but the system calibration is relatively complex.

7. Meta-Sensing

Meta-sensing primarily relies on the phase and polarization manipulation capabilities of metamaterial structures. It achieves micro-nano multiphysics coupling through the localization and structural response characteristics of multiphysics fields, such as label-free biomolecule recognition, multidirectional tactile sensing, and sub-piconewton force/torque detection. It exhibits unique advantages in human–machine interaction, biomedical diag-

nostics, and optomechanical manipulation, becoming an important pathway to overcome the performance bottlenecks of precision measurement [126,127]. Zeng et al. used digital embroidery technology to prepare a flexible metamaterial biosensor (Figure 10a). Through near-field interaction between wireless signals and the human body, non-contact continuous monitoring of cardiopulmonary signals was achieved in kinetic environments such as aircraft cabin simulators, demonstrating the practical application potential of metamaterials in wearable biomedical sensing [128]. Inspired by the dendritic three-dimensional structure of human skin, Zhang et al. used 3D printing technology to construct a piezoresistive metamaterial with multi-directional sensing capabilities. By controlling the distribution of different lattice micro-units, a multi-directional and multi-functional force-sensitive response was achieved, providing a new sensing platform for flexible wearable devices and intelligent human–computer interaction (Figure 10b) [129]. Hong et al. used tunable elliptical cylindrical metamaterial structures, as shown in Figure 10c, and combined them with single-molecule rotational mechanics measurement technology to achieve real-time monitoring of the rotational dynamics of a single biomolecule [130]. Peng et al. designed Si/Si_3N_4 (SSN) multilayer metamaterial nanoparticles (Figure 10d) that can be used as optical trapping probes through deep learning methods, which significantly improved the trapping stiffness of optical tweezers [131].

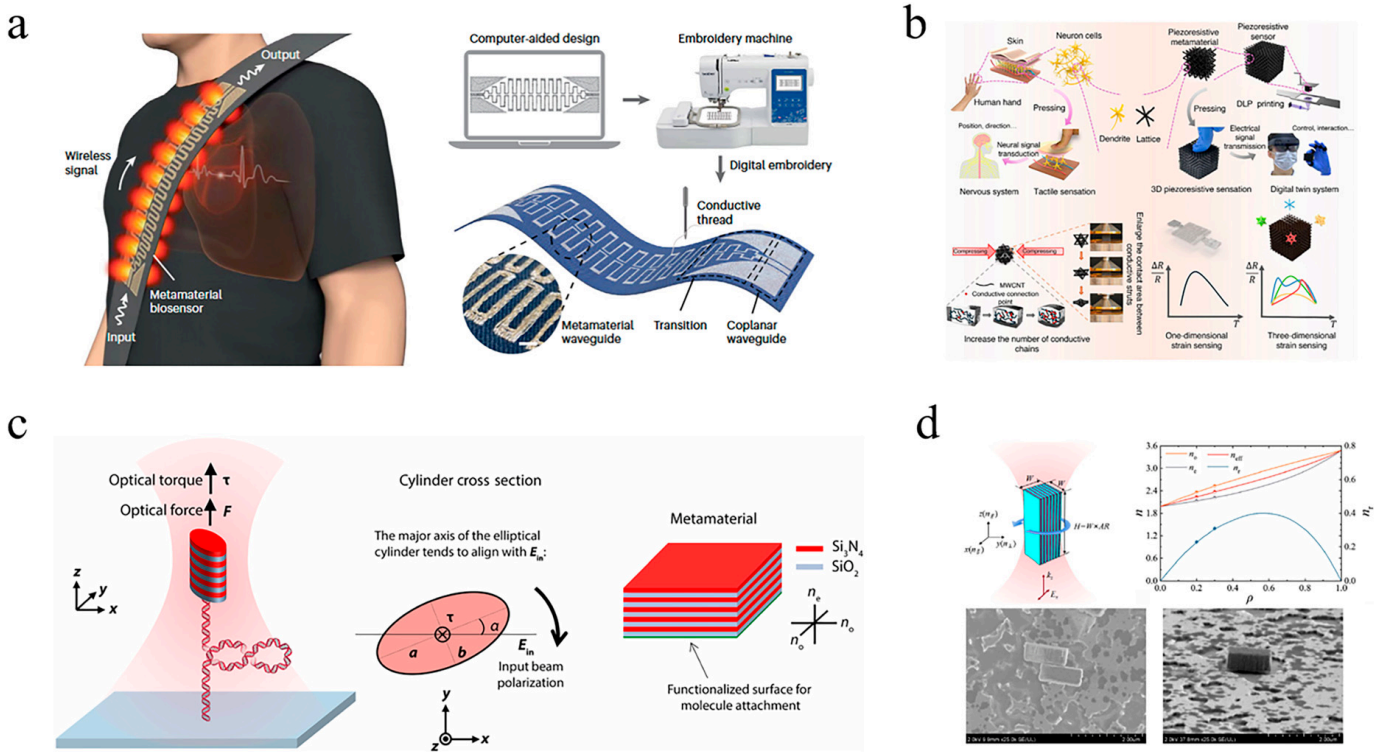


Figure 10. Meta-sensing. (**a**) Contactless metamaterial biosensor [128]. (**b**) Dendrite-mimicked 3D piezoresistive metamaterials with directional sensation manufactured via DLP-based 3D printing [129]. (**c**) Working principle of metamaterial elliptical cylinders in AOT [130]. (**d**) SSN nanoparticles as optical trapping probes [131].

These research schemes each have their own focus. Flexible metamaterial sensors are good at wearable non-contact detection but have limited environmental stability [128]; 3D-printed piezoresistive metamaterials achieve multi-directional force-sensitive response but face miniaturization challenges [129]; single-molecule mechanical manipulation has extremely high precision, but the system is complex [130]; deep learning-assisted optical

capture probes have excellent stiffness, but their data dependence and fabrication tolerance are still bottlenecks [131].

In short, meta-sensing, by integrating metamaterial design, advanced micro/nano manufacturing and intelligent algorithms, not only expands the sensing dimension and detection limit but also promotes the breakthrough of sensing technology towards flexibility, precision and multifunctional integration, providing core support for the cross-domain application and performance upgrade of high-end sensing equipment.

8. Conclusions

With its novel physical concepts and theoretical foundations that break through the traditional optical framework, meta-optics has paved a new path for the extreme miniaturization, high integration, and multifunctionality of optical components. Metasurfaces, as the core platform of meta-optics, enable end-to-end control of light, from basic wavefront modulation to complex optical calculations [32,67,68]. In fact, relying on the precise coordinated manipulation of the phase, amplitude, and polarization of the light field, various meta-devices and their applications in multi-dimensional parallel manipulation of light fields have demonstrated superior characteristics that disrupt traditional optical systems [34,42,53]. This paper systematically reviews the core physical mechanisms of meta-optics, typical meta-devices, and their latest research results in waveguide integration, laser manipulation, spectral detection and sensor detection. It elaborates on the fundamental principles and implementation methods of optical field manipulation, and focuses on the design concepts and key applications of core devices such as meta-waveguides (planar and fiber-type), meta-lasers, meta-spectrometers and meta-sensing [80,91,109,124,125,127,128].

However, the future development and industrial application of metadevices still face many critical challenges that urgently need to be addressed. In integrated design, the precise alignment of subwavelength-scale meta-atoms places stringent requirements on micro/nano fabrication processes and device operation [45,80]. While all-dielectric metasurfaces achieve efficient control of the optical field, their broadband achromatic performance is still limited by both physical mechanisms and manufacturing processes [19,36]. With the increase in numerical aperture and operating bandwidth of metadevices, the design requirements for high aspect ratio meta-atoms are constantly increasing, and the controllable fabrication of high aspect ratio meta-atoms remains a challenge in the current micro/nano fabrication field [80,101]. Simultaneously, the response speed and modulation efficiency of dynamically reconfigurable metadevices are difficult to balance, and the problems of ohmic loss and modulation delay have not been fundamentally solved [47,112]. Furthermore, the integrated packaging of on-chip metadevices is crucial, but the near-field coupling between the packaging material and the metasurface easily leads to a decrease in device modulation efficiency, becoming a significant obstacle to the practical application of on-chip integrated systems [82].

To systematically evaluate the advantages and disadvantages of metasurface devices, we conduct a multi-dimensional comparison with traditional integrated optical devices. In terms of bandwidth, traditional waveguide devices, based on total internal reflection or slow light effects, can support broadband operation on the order of hundreds of nanometers, while the bandwidth of resonant metasurface devices is limited by their intrinsic quality factor and is typically narrower [12,41]. From a manufacturing process perspective, metasurface devices rely on high-precision micro-nano fabrication technologies such as electron beam lithography, resulting in significantly higher manufacturing costs and process complexity compared to waveguide devices fabricated using traditional photolithography [89,126]. Regarding optical losses, the propagation loss of all-dielectric metasurfaces has been reduced to a level comparable to that of traditional silicon waveguides, while

plasmonic metasurfaces are still plagued by ohmic losses [77,85]. In terms of integration density, metasurfaces can integrate multiple independent functions on the subwavelength scale, achieving a functional density per unit area far exceeding that of traditional photonic integrated circuits composed of discrete components [16,41,75]. Therefore, metasurface devices have significant advantages in integration density and multifunctional integration but still face challenges in broadband response and low-cost mass production. Future research needs to find the optimal trade-off among these performance indicators.

With the continuous development of light field manipulation technology and the continuous breakthroughs in micro-nano fabrication processes, the research focus of meta-optics is gradually extending to interdisciplinary frontier fields, and the exploration results in novel light field manipulation and cutting-edge optical applications are exciting. For example, the nonlocal manipulation mechanism based on continuous domain bound states provides a new path for meta-devices to achieve high Q-value resonance and precise control of chiral light fields [66,69]; the design and realization of on-chip topological metasurfaces have successfully integrated topological photonics with meta-optics, laying the foundation for highly robust optical information transmission and holographic display [82,100]; dynamic meta-devices based on MEMS and graphene have realized rapid switching of light field modes and electric drive control of complex amplitudes, providing an effective solution for the development of reconfigurable optoelectronic devices [47,112]; the combination of meta-fibers and 3D nanoprinting technology has broken through the functional limitations of traditional optical fibers, realizing complex light field manipulation such as remote focusing and achromatic imaging [98,101]; meta-spectrometer, by utilizing the powerful optical field manipulation capabilities of subwavelength structures, breaks through the performance and size bottlenecks of traditional spectrometers in terms of miniaturization and on-chip integration, providing a completely new solution for portable, high-sensitivity spectral analysis [122,124]; meta-sensing technology has made significant progress in fields such as biomedicine, human–computer interaction, and precision measurement, providing new solutions for high-sensitivity and multifunctional sensing [126–131]. These studies have not only enriched the physical connotation of meta-optics but also provided new ideas for the integration and innovation of meta-optics and traditional photonics [29,77].

The continuous innovation of novel physical concepts, the deepening of light field manipulation principles, and the gradual expansion of key applications have enabled meta-optics to maintain its vigorous development. With the dual support of metasurface physical mechanisms and vector light field manipulation technology, we envision that the research focus of meta-optics will be on three major directions: exploring the physical limits of light field manipulation and tapping the application potential of new effects such as non-Hermitian physics and topological photonics in meta-devices [85,109]; achieving the integration of multifunctional computational imaging, parallel image processing, spectral detection and sensing at the chip scale, promoting the standardized application of meta-waveguides, meta-lasers, meta-spectrometers and meta-sensing in on-chip photonic systems [80,83]; and continuously improving the working efficiency and bandwidth of meta-devices, breaking through the dual limitations of fabrication process and physical mechanism, and accelerating the industrialization process of meta-optical devices. This development trend will drive meta-optics from basic research to practical application, providing core technical support for the next generation of miniaturized, integrated, and intelligent photonic systems [29,109]. Research in meta-optics will further explore two interdisciplinary directions: optical force manipulation and quantum photonics. The principles and applications of optical force manipulation based on advanced nanophotonic structures have been systematically elucidated [132]. The reversible transverse optical force of phase-gradient metasurfaces [133] and the polarization-dependent optical force of Fano

interference [134] provide new pathways for optical manipulation and optical tweezers applications in meta-devices. Meanwhile, metasurface-assisted multimode quantum imaging has opened up a new direction for the integration of meta-optics and quantum photonics, becoming an important research hotspot for future metaphotonic devices.

Author Contributions: Conceptualization, Y.L.; writing—original draft preparation, H.Z.; writing—review and editing, H.Z., Z.D., Y.Z., Y.H., J.W., Z.C., Y.G. and J.H.; visualization, Y.L.; supervision, Y.L.; project administration, Y.L.; funding acquisition, Y.L. All authors have read and agreed to the published version of the manuscript.

Funding: This research was funded by the Talent Project Scientific Research Foundation for High-level Talents of Anhui University of Technology (QD202378, QD202306); the National Natural Science Foundation of China (62505002); the Natural Science Foundation of Anhui University of Technology (QZ202420); the College Students Innovative Entrepreneurial Training Plan Program of Anhui University of Technology (202410360089, 202510360082); and the Natural Science Research Project of Anhui Educational Committee (2024AH050168).

Data Availability Statement: No new data was created.

Acknowledgments: The authors thank the help from Yu Lei 's support.

Conflicts of Interest: The authors have no conflicts to disclose.

References

1. Qiu, X.; Li, F.; Zhang, W.; Zhu, Z.-H.; Chen, L. Spiral phase contrast imaging in nonlinear optics: Seeing phase objects using invisible illumination. *Optica* **2018**, *5*, 208–212. [CrossRef]
2. Qiu, X.; Zhang, D.; Zhang, W.; Chen, L. Structured-Pump-Enabled Quantum Pattern Recognition. *Phys. Rev. Lett.* **2019**, *122*, 123901. [CrossRef]
3. Qiu, X.; Guo, H.; Chen, L. Remote transport of high-dimensional orbital angular momentum states and ghost images via spatial-mode-engineered frequency conversion. *Nat. Commun.* **2023**, *14*, 8244. [CrossRef]
4. Su, X.; Qiu, X.; Wang, J.; Zhang, D.; Hong, L.; Lin, F.; Fu, S.; Ren, Y.; Chen, L. Seeing Trajectory Without Imaging by Exploring Both Radial Momentum and Orbital Angular Momentum of Light. *Laser Photonics Rev.* **2026**, e02894. [CrossRef]
5. Yu, Z.; Li, X. Metasurfaces for full-parameter optical wavefront engineering. *Light Adv. Manuf.* **2026**, *7*, 10. [CrossRef]
6. Chen, L.; You, J.W.; Ma, Q.; Su, J.L.; Qin, S.L.; Peng, Q.C.; Xiao, Q.; Cui, T.J. Quantum-inspired superposition and nonseparable states of reconfigurable metasurfaces in classical systems. *Nat. Commun.* **2026**, *17*, 560. [CrossRef]
7. Jahani, S.; Jacob, Z. All-dielectric metamaterials. *Nat. Nanotechnol.* **2016**, *11*, 23–36. [CrossRef] [PubMed]
8. Kildishev, A.V.; Boltasseva, A.; Shalaev, V.M. Planar photonics with metasurfaces. *Science* **2013**, *339*, 1232009. [CrossRef] [PubMed]
9. Li, T.; Fu, B.; Ren, J.; Wang, S.; Wang, Z.; Zhu, S. Multidimensional light field manipulation and applications based on optical metasurface. In *First Optics Frontier Conference*; SPIE: Bellingham, WA, USA, 2021; Volume 11850, pp. 11–15.
10. Li, T.; Xu, X.; Fu, B.; Wang, S.; Li, B.; Wang, Z.; Zhu, S. Integrating the optical tweezers and spanner onto an individual single-layer metasurface. *Photonics Res.* **2021**, *9*, 1062–1068. [CrossRef]
11. Zheng, S.; Yu, Y.; Zhou, X.; Fu, B.; Wang, S.; Wang, Z.; Zhu, S. Research on multidimensional optical imaging empowered by metasurfaces (Invited). *Laser Optoelectron. Prog.* **2024**, *61*, 1611001.
12. Fu, B.; Zou, X.; Li, T.; Wang, S.; Wang, Z.; Zhu, S. Review: Chromatic dispersion manipulation based on optical metasurfaces. *J. Harbin Inst. Technol.* **2020**, *27*, 1–19.
13. Fu, B.; Bi, Q.; Zheng, S.; Peng, Y.; Wang, S.; Cao, X.; Wang, Z.; Zhu, S. Advanced metasurface imaging and display based on multidimensional light field manipulation (Invited). *Acta Opt. Sin.* **2024**, *44*, 1400001.
14. Lin, R.-Y.; Wu, Y.-F.; Fu, B.-Y.; Wang, S.-M.; Wang, Z.-L.; Zhu, S.-N. Application of chromatic aberration control of metalens. *Chin. Opt.* **2021**, *14*, 764–781. [CrossRef]
15. Liu, M.; Li, T.; Ge, Q.; Wang, S.; Wang, Z.; Zhu, S. Phase modulation mechanism and research progress of multifunctional metasurfaces. *Acta Opt. Sin.* **2022**, *42*, 2126004.
16. Li, H.; Zhao, C.; Li, J.; Xu, H.; Xu, W.; Tan, Q.; Song, C.; Shen, Y.; Yao, J. Spin-dependent amplitude and phase modulation with multifold interferences via single-layer diatomic all-silicon metasurfaces. *Opto-Electron. Sci.* **2025**, *4*, 240025. [CrossRef]
17. Zhang, X.; Liu, Z. Superlenses to overcome the diffraction limit. *Nat. Mater.* **2008**, *7*, 435–441. [CrossRef] [PubMed]
18. Khorasaninejad, M.; Chen, W.T.; Devlin, R.C.; Oh, J.; Zhu, A.Y.; Capasso, F. Metalenses at visible wavelengths: Diffraction-limited focusing and subwavelength resolution imaging. *Science* **2016**, *352*, 1190–1194. [CrossRef] [PubMed]

19. Wang, S.; Wu, P.C.; Su, V.-C.; Lai, Y.-C.; Chen, M.-K.; Kuo, H.Y.; Chen, B.H.; Chen, Y.H.; Huang, T.-T.; Wang, J.-H. A broadband achromatic metalens in the visible. *Nat. Nanotechnol.* **2018**, *13*, 227–232. [CrossRef]
20. Zhao, R.; Sain, B.; Wei, Q.; Tang, C.; Li, X.; Weiss, T.; Huang, L.; Wang, Y.; Zentgraf, T. Multichannel vectorial holographic display and encryption. *Light Sci. Appl.* **2018**, *7*, 95. [CrossRef]
21. Li, T.; Gao, W.; Fu, B.; Shao, T.; Fu, Y.; Zavatski, S.; Nayak, J.K.; Yan, S.; Xu, X.; Wang, S.; et al. Scalable generalized meta-spanners enabling parallel multitasking optical manipulation. *Sci. Adv.* **2026**, *12*, eaed5302. [CrossRef] [PubMed]
22. Ren, H.; Shao, W.; Li, Y.; Gu, M. Three-dimensional vectorial holography based on machine learning inverse design. *Sci. Adv.* **2020**, *6*, eaaz4261. [CrossRef]
23. Bao, Y.; Yu, Y.; Xu, H.; Guo, C.; Li, J.; Sun, S.; Zhou, Z.-K.; Qiu, C.-W.; Wang, X.-H. Full-colour nanoprint-holographic synchronous metasurface with arbitrary hue saturation and brightness control. *Light Sci. Appl.* **2019**, *8*, 95. [CrossRef]
24. Xu, X.; Gao, W.; Li, T.; Shao, T.; Li, X.; Zhou, Y.; Gao, G.; Wang, G.; Yan, S.; Wang, S.; et al. Metasurfaces-empowered optical micromanipulation (Invited). *Acta Opt. Sin.* **2024**, *44*, 0500001.
25. Lin, J.; Qiu, M.; Zhang, X.; Guo, H.; Cai, Q.; Xiao, S.; He, Q.; Zhou, L. Tailoring the lineshapes of coupled plasmonic systems based on a theory derived from first principles. *Light Sci. Appl.* **2020**, *9*, 158. [CrossRef]
26. Xiao, Q.; Fan, L.H.; Ma, Q.; Ning, Y.M.; Gu, Z.; Chen, L.; Li, L.; You, J.W.; Niu, Y.F.; Cui, T.J. Secure wireless communication of brain–computer interface and mind control of smart devices enabled by space-time-coding metasurface. *Nat. Commun.* **2025**, *16*, 7914. [CrossRef] [PubMed]
27. Xiao, Q.; Gao, W.; Ma, Q.; Gu, Z.; Zhou, Y.; Liu, C.; Huang, Z.A.; Wan, X.; Li, L.; Li, Y.; et al. Electromagnetic brain–computer–metasurface holography. *ACS Photonics* **2023**, *10*, 2249–2256. [CrossRef]
28. Ning, Y.M.; Ma, Q.; Xiao, Q.; Gao, X.X.; Wu, Q.W.; Gu, Z.; Li, R.S.; Chen, L.; You, J.W.; Cui, T.J. Multilayer nonlinear diffraction neural networks with programmable and fast ReLU activation function. *Nat. Commun.* **2025**, *16*, 10332. [CrossRef]
29. Zhang, J.C.; Wu, G.-B.; Chen, M.K.; Liu, X.; Chan, K.F.; Tsai, D.P.; Chan, C.H. A 6G meta-device for 3D varifocal. *Sci. Adv.* **2023**, *9*, eadf8478. [CrossRef]
30. Zhou, Y.; Zhu, X.; Li, T.; Zhou, Z.; Bi, Q.; Liu, J.; Chen, J.; Fu, B.; He, J.; Feng, X. Metasurface-assisted multimodal quantum imaging. *Proc. Natl. Acad. Sci. USA* **2025**, *122*, e2500760122. [CrossRef]
31. Ou, K.; Wan, H.; Wang, G.; Zhu, J.; Dong, S.; He, T.; Yang, H.; Wei, Z.; Wang, Z.; Cheng, X. Advances in meta-optics and metasurfaces: Fundamentals and applications. *Nanomaterials* **2023**, *13*, 1235. [CrossRef]
32. Yu, N.; Genevet, P.; Kats, M.A.; Aieta, F.; Tetienne, J.-P.; Capasso, F.; Gaburro, Z. Light propagation with phase discontinuities: Generalized laws of reflection and refraction. *Science* **2011**, *334*, 333–337. [CrossRef]
33. Zhou, S.; Li, L.; Gao, L.; Zhou, Z.; Yang, J.; Zhang, S.; Wang, T.; Gao, C.; Fu, S. Hybrid strategy in compact tailoring of multiple degrees-of-freedom toward high-dimensional photonics. *Light Sci. Appl.* **2025**, *14*, 167. [CrossRef]
34. Deng, Z.-L.; Li, G. Metasurface optical holography. *Mater. Today Phys.* **2017**, *3*, 16–32. [CrossRef]
35. Li, S.; Tsakmakidis, K.L.; Jiang, T.; Shen, Q.; Zhang, H.; Yan, J.; Sun, S.; Shen, L. Unidirectional guided-wave-driven metasurfaces for arbitrary wavefront control. *Nat. Commun.* **2024**, *15*, 5992. [CrossRef] [PubMed]
36. Khorasaninejad, M.; Ambrosio, A.; Kanhaiya, P.; Capasso, F. Broadband and chiral binary dielectric meta-holograms. *Sci. Adv.* **2016**, *2*, e1501258. [CrossRef]
37. Qiu, X.; Zhang, J.; Fan, Y.; Zhou, J.; Chen, L.; Tsai, D.P. Metasurface enabled high-order differentiator. *Nat. Commun.* **2025**, *16*, 2437. [CrossRef]
38. Zhang, J.C.; Yao, J.; Tsai, D.P. Meta-lens based on multi-level phase-change. *J. Appl. Phys.* **2024**, *136*, 053101. [CrossRef]
39. Sun, Z.; Li, T.; Kuang, S.; Yun, X.; He, M.; Fu, B.; Fu, Y.; Zhao, T.; Wang, S.; Liang, Y. On-demand quick metasurface design with neighborhood attention transformer. *arXiv* **2024**, arXiv:2412.08405. [CrossRef]
40. Zhang, J.; Pang, X.; Ding, J. Wavefront spacing and Gouy phase in strongly focused fields: The role of polarization. *J. Opt. Soc. Am. A* **2017**, *34*, 1132–1138. [CrossRef]
41. Zhang, J.C.; Wu, G.-B.; Chen, M.K.; Che, X.; Liang, Y.; Tsai, D.P.; Chan, C.H. Electromagnetic wave tailoring: From one dimension to multiple dimensions. *Electromagn. Sci.* **2023**, *1*, 0030131. [CrossRef]
42. Cong, D.; Feng, H.; Wang, S.; Wang, T.; Zhao, R.; Gao, Y. Dual-wavelength terahertz metasurface capable of amplitude and phase modulation for wavefront manipulation and holography. *J. Appl. Phys.* **2025**, *138*, 103103. [CrossRef]
43. Dorrah, A.H.; Park, J.-S.; Palmieri, A.; Capasso, F. Free-standing bilayer metasurfaces in the visible. *Nat. Commun.* **2025**, *16*, 3126. [CrossRef]
44. Ouyang, X.; Zeng, Y.; Wang, Z.; Bo, B.; Lai, F.; Zhang, C.; Qiu, C.-w.; Song, Q.; Yu, S.; Kivshar, Y. Ultra narrowband geometric-phase resonant metasurfaces. *Proc. Natl. Acad. Sci. USA* **2025**, *122*, e2420830122. [CrossRef]
45. Xu, C.; Ren, Z.; Zhou, H.; Zhou, J.; Li, D.; Lee, C. Near-field coupling induced less chiral responses in chiral metamaterials for surface-enhanced vibrational circular dichroism. *Adv. Funct. Mater.* **2024**, *34*, 2314482. [CrossRef]
46. Boroviks, S.; Martin, O.J.F. Monocrystalline gold Metasurface to control anisotropic second-harmonic generation. *Adv. Opt. Mater.* **2025**, *13*, 2570090. [CrossRef]

47. Han, S.; Kim, S.; Kim, S.; Low, T.; Brar, V.W.; Jang, M.S. Complete complex amplitude modulation with electronically tunable graphene plasmonic metamolecules. *ACS Nano* **2020**, *14*, 1166–1175. [CrossRef]
48. Overvig, A.C.; Shrestha, S.; Malek, S.C.; Lu, M.; Stein, A.; Zheng, C.; Yu, N. Dielectric metasurfaces for complete and independent control of the optical amplitude and phase. *Light Sci. Appl.* **2019**, *8*, 92. [CrossRef]
49. Ren, J.; Li, T.; Fu, B.; Wang, S.; Wang, Z.; Zhu, S. Wavelength-dependent multifunctional metalens devices via genetic optimization. *Opt. Mater. Express* **2021**, *11*, 3908–3916. [CrossRef]
50. Zhang, J.C.; Chen, M.K.; Fan, Y.; Chen, Q.; Chen, S.; Yao, J.; Liu, X.; Xiao, S.; Tsai, D.P. Miniature tunable Airy beam optical meta-device. *Opto-Electron. Adv.* **2024**, *7*, 230171. [CrossRef]
51. Zhang, J.C.; Fan, Y.; Yao, J.; Chen, M.K.; Lin, S.; Liang, Y.; Leng, B.; Tsai, D.P. Programmable optical meta-holograms. *Nanophotonics* **2024**, *13*, 1201–1217. [CrossRef] [PubMed]
52. Li, T.; Chen, Y.; Fu, B.; Liu, M.; Wang, J.; Gao, H.; Wang, S.; Zhu, S. Spin-selective trifunctional metasurfaces for deforming versatile nondiffractive beams along the optical trajectory. *Laser Photonics Rev.* **2024**, *18*, 2301372. [CrossRef]
53. Arbabi, A.; Horie, Y.; Bagheri, M.; Faraon, A. Dielectric metasurfaces for complete control of phase and polarization with subwavelength spatial resolution and high transmission. *Nat. Nanotechnol.* **2015**, *10*, 937–943. [CrossRef]
54. Tan, L.; Huo, P.; Lin, P.; Ren, Y.; Qi, H.; Fang, L.; Wang, Y.; Ou, J.; Lu, Y.; Xu, T. Longitudinally engineered metasurfaces for 3D vectorial holography. *Light Sci. Appl.* **2026**, *15*, 36. [CrossRef]
55. Fan, Q.; Liu, M.; Zhang, C.; Zhu, W.; Wang, Y.; Lin, P.; Yan, F.; Chen, L.; Lezec, H.J.; Lu, Y.; et al. Independent amplitude control of arbitrary orthogonal states of polarization via dielectric metasurfaces. *Phys. Rev. Lett.* **2020**, *125*, 267402. [CrossRef]
56. Song, Q.; Baroni, A.; Sawant, R.; Ni, P.; Brandli, V.; Chenot, S.; Vézian, S.; Damilano, B.; de Mierry, P.; Khadir, S.; et al. Ptychography retrieval of fully polarized holograms from geometric-phase metasurfaces. *Nat. Commun.* **2020**, *11*, 2651. [CrossRef]
57. Rubin, N.A.; Shi, Z.; Capasso, F. Polarization in diffractive optics and metasurfaces. *Adv. Opt. Photonics* **2021**, *13*, 836–970. [CrossRef]
58. Wang, J.; Chen, J.; Yu, F.; Chen, R.; Wang, J.; Zhao, Z.; Li, X.; Xing, H.; Li, G.; Chen, X.; et al. Unlocking ultra-high holographic information capacity through nonorthogonal polarization multiplexing. *Nat. Commun.* **2024**, *15*, 6284. [CrossRef] [PubMed]
59. Wang, Z.-Q.; Li, F.-J.; Deng, Q.-M.; Wan, Z.; Li, X.; Deng, Z.-L. Inverse-designed Jones matrix metasurfaces for high-performance meta-polarizers. *Chin. Opt. Lett.* **2024**, *22*, 023601. [CrossRef]
60. Fu, B.; Zhou, X.; Li, T.; Zhu, H.; Liu, Z.; Zheng, S.; Zhou, Y.; Yu, Y.; Cao, X.; Wang, S. Miniaturized high-efficiency snapshot polarimetric stereoscopic imaging. *Optica* **2025**, *12*, 391–398. [CrossRef]
61. Li, T.; Li, X.; Yan, S.; Xu, X.; Wang, S.; Yao, B.; Wang, Z.; Zhu, S. Generation and conversion dynamics of dual Bessel beams with a photonic spin-dependent dielectric metasurface. *Phys. Rev. Appl.* **2021**, *15*, 014059. [CrossRef]
62. Zhang, J.C.; Chen, M.K.; Liang, Y.; Hong, X.; Wang, M.; Cheng, Y.; Liu, X.; Tsai, D.P.; Pang, S.W. Nanoimprint meta-device for chiral imaging. *Adv. Funct. Mater.* **2023**, *33*, 2306422. [CrossRef]
63. Zhang, Z.; Kuang, C.; Zang, H.; Lu, Y.; Wang, P. Simultaneously detecting transversal and longitudinal displacement with the dielectric metasurface. *Chin. Opt. Lett.* **2024**, *22*, 021202. [CrossRef]
64. Overvig, A.; Alù, A. Diffractive Nonlocal Metasurfaces. *Laser Photonics Rev.* **2022**, *16*, 2100633. [CrossRef]
65. Zhang, J.C.; Tsai, D.P.; Pang, S.W. Non-local bound states in the continuum for nanoscale alignment. *Nat. Photonics* **2026**, *20*, 296–300. [CrossRef]
66. Hsu, C.W.; Zhen, B.; Stone, A.D.; Joannopoulos, J.D.; Soljačić, M. Bound states in the continuum. *Nat. Rev. Mater.* **2016**, *1*, 16048. [CrossRef]
67. Hsu, C.W.; Zhen, B.; Lee, J.; Chua, S.-L.; Johnson, S.G.; Joannopoulos, J.D.; Soljačić, M. Observation of trapped light within the radiation continuum. *Nature* **2013**, *499*, 188–191. [CrossRef]
68. Koshelev, K.; Lepeshov, S.; Liu, M.; Bogdanov, A.; Kivshar, Y. Asymmetric metasurfaces with high-Q resonances governed by bound states in the continuum. *Phys. Rev. Lett.* **2018**, *121*, 193903. [CrossRef]
69. Qin, H.; Su, Z.; Liu, M.; Zeng, Y.; Tang, M.-C.; Li, M.; Shi, Y.; Huang, W.; Qiu, C.-W.; Song, Q. Arbitrarily polarized bound states in the continuum with twisted photonic crystal slabs. *Light Sci. Appl.* **2023**, *12*, 66. [CrossRef]
70. Chen, R.; Bi, Q.; Li, T.; Wang, S.; Zhu, S.; Wang, Z. Dual-wavelength chiral metasurfaces based on quasi-bound states in the continuum. *J. Opt.* **2023**, *25*, 045001. [CrossRef]
71. Chen, R.; Li, T.; Bi, Q.; Wang, S.; Zhu, S.; Wang, Z. Quasi-bound states in the continuum-based switchable light-field manipulator. *Opt. Mater. Express* **2022**, *12*, 1232–1241. [CrossRef]
72. Li, T.; Liu, M.; Qin, J.; Ren, J.; Hou, J.; Liu, Y.; Yang, X.; Chu, H.; Lai, Y.; Wang, S. Configurable topological photonic polycrystal based on a synthetic hybrid dimension. *Natl. Sci. Rev.* **2025**, *12*, nwaf107. [CrossRef]
73. Li, H.; Li, T.; Zhang, J. Practically reliable high-Q guided-mode resonances via coupler-assisted BICs. *Opt. Express* **2026**, *34*, 13133–13141. [CrossRef]
74. Moretti, G.Q.; Tittl, A.; Cortés, E.; Maier, S.A.; Bragas, A.V.; Grinblat, G. Introducing a symmetry-breaking coupler into a dielectric metasurface enables robust high-Q quasi-BICs. *Adv. Photonics Res.* **2022**, *3*, 2200111. [CrossRef]

75. Chen, H.-T.; Taylor, A.J.; Yu, N. A review of metasurfaces: Physics and applications. *Rep. Prog. Phys.* **2016**, *79*, 076401. [CrossRef]
76. Li, S.; Gao, Y.; Guo, R.; Yao, S.; Hu, J.; Lei, Y. Metasurface-enabled on-chip manipulation for light focusing and modes recognition. *Opt. Commun.* **2025**, *520*, 132033. [CrossRef]
77. Khorasaninejad, M.; Capasso, F. Metalenses: Versatile multifunctional photonic components. *Science* **2017**, *358*, eaam8100. [CrossRef] [PubMed]
78. Sırmacı, Y.D.; Gomez, A.B.; Pertsch, T.; Schmid, J.H.; Cheben, P.; Staude, I. All-Dielectric Huygens' meta-waveguides for resonant integrated photonics. *Laser Photonics Rev.* **2023**, *17*, 2200860. [CrossRef]
79. Cui, W.Y.; Zhang, J.; Luo, Y.; Gao, X.; Cui, T.J. Dynamic switching from coherent perfect absorption to parametric amplification in a nonlinear spoof plasmonic waveguide. *Nat. Commun.* **2024**, *15*, 2824. [CrossRef]
80. Wang, J.; Wang, W.; Ding, W.; Lin, J.; Jin, P.; Liu, S.; Zhou, K. All-dielectric meta-waveguides for on-chip integration. *npj Nanophotonics* **2025**, *2*, 20. [CrossRef]
81. Chen, T.; Xu, M.; Pu, M.; Zeng, Q.; Zheng, Y.; Xiao, Y.; Ha, Y.; Guo, Y.; Zhang, F.; Chi, N.; et al. Freeform Metasurface-assisted waveguide coupler for guided wave polarization manipulation and spin−orbit angular momentum conversion. *ACS Photonics* **2024**, *11*, 1051−1059. [CrossRef]
82. Ji, J.; Li, J.; Wang, Z.; Li, X.; Sun, J.; Wang, J.; Fang, B.; Chen, C.; Ye, X.; Zhu, S.; et al. On-chip multifunctional metasurfaces with full-parametric multiplexed Jones matrix. *Nat. Commun.* **2024**, *15*, 8271. [CrossRef] [PubMed]
83. Yi, C.; Wang, Z.; Shi, Y.; Wan, S.; Tang, J.; Hu, W.; Li, Z.; Zeng, Y.; Song, Q.; Li, Z. Creating topological exceptional point by on-chip all-dielectric metasurface. *Light Sci. Appl.* **2025**, *14*, 262. [CrossRef] [PubMed]
84. Shi, Y.; Wan, S.; Wang, Z.; Rao, R.; Li, Z. On-chip nonlocal metasurface for color router: Conquering efficiency-loss from spatial-multiplexing. *Light Sci. Appl.* **2026**, *15*, 66. [CrossRef]
85. Li, T.; Liu, M.; Hou, J.; Yang, X.; Wang, S.; Wang, S.; Zhu, S.; Tsai, D.P.; Wang, Z. Chip-scale metaphotonic singularities: Topological, dynamical, and practical aspects. *Chip* **2024**, *3*, 100109. [CrossRef]
86. Xiong, Y.; Chen, J.; Lu, Y.; Xu, F. Broadband optical-fiber compatible photodetector based on a graphene-MoS2-WS2 heterostructure with a synergetic photogenerating mechanism. *Adv. Electron. Mater.* **2019**, *5*, 1800562. [CrossRef]
87. Xiong, Y.; Wang, Y.; Zhu, R.; Xu, H.; Wu, C.; Chen, J.; Ma, Y.; Liu, Y.; Chen, Y.; Watanabe, K.; et al. Twisted black phosphorus-based van der Waals stacks for fiber-integrated polarimeters. *Sci. Adv.* **2022**, *8*, eabo0375. [CrossRef]
88. Xiong, Y.; Xu, H.; Wang, Y.; Wu, C.; Ding, Z.; Chen, M.; Hao, Y.; Chen, Y.; Xu, F. An ultracompact multicore fiber de-multiplexer by endface-integrating graphene photodetector array. *ACS Photonics* **2022**, *9*, 1808–1813. [CrossRef]
89. Xiong, Y.; Xu, F. Multifunctional integration on optical fiber tips: Challenges and opportunities. *Adv. Photonics* **2020**, *2*, 064001. [CrossRef]
90. Lei, Y.; Xiong, Y.; Xu, F.; Chen, Z. Metasurface around the side surface of optical fiber for light focusing. *Opt. Express* **2022**, *30*, 40916–40924. [CrossRef]
91. Hua, H.; Zeng, C.; He, Z.; Lu, H.; Du, Y.; Mao, D.; Zhao, J. Plasmonic metafiber for all-fiber Q-switched cylindrical vector lasers. *Nanophotonics* **2023**, *12*, 725–735. [CrossRef] [PubMed]
92. Li, C.; Wieduwilt, T.; Wendisch, F.J.; Márquez, A.; Menezes, L.S.; Maier, S.A.; Schmidt, M.A.; Ren, H. Metafiber transforming arbitrarily structured light. *Nat. Commun.* **2023**, *14*, 7222. [CrossRef]
93. Fang, X.; Yang, H.; Yao, W.; Wang, T.; Zhang, Y.; Gu, M.; Xiao, M. High-dimensional orbital angular momentum multiplexing nonlinear holography. *Adv. Photonics* **2021**, *3*, 015001. [CrossRef]
94. Zhao, Q.; Zhou, J.; Zhang, F.; Lippens, D. Mie resonance-based dielectric metamaterials. *Mater. Today* **2009**, *12*, 60–69. [CrossRef]
95. Zhou, Z.; Li, J.; Su, R.; Yao, B.; Fang, H.; Li, K.; Zhou, L.; Liu, J.; Stellinga, D.; Reardon, C.P.; et al. Efficient silicon metasurfaces for visible light. *ACS Photonics* **2017**, *4*, 544–551. [CrossRef]
96. Ha, S.T.; Fu, Y.H.; Emani, N.K.; Pan, Z.; Bakker, R.M.; Paniagua-Domínguez, R.; Kuznetsov, A.I. Directional lasing in resonant semiconductor nanoantenna arrays. *Nat. Nanotechnol.* **2018**, *13*, 1042–1047. [CrossRef] [PubMed]
97. Xu, H.; Li, T.; Gao, G.; Fang, S.; Liu, H.; Ding, H.; Chen, X.; Xiong, Y.; Wang, S.; Xu, F. Metasurface-integrated pattern-preserved fiber Mode Separator. *Adv. Funct. Mater.* **2025**, *35*, 2505081. [CrossRef]
98. Khosravi, M.; Wieduwilt, T.; Zeisberger, M.; Lorenz, A.; Schmidt, M.A. Advanced remote focus control in multicore meta-fibers through 3D nanoprinted phase-only holograms. *Nat. Commun.* **2025**, *16*, 507. [CrossRef]
99. Sun, J.; Huang, W.; Lorenz, A.; Zeisberger, M.; Schmidt, M.A. Tunable metafibers: Remote spatial focus control using 3D nanoprinted holograms on dual-core fibers. *Light Sci. Appl.* **2025**, *14*, 237. [CrossRef]
100. He, T.; Meng, Y.; Wang, L.; Zhong, H.; Mata-Cervera, N.; Li, D.; Yan, P.; Liu, Q.; Shen, Y.; Xiao, Q. Optical skyrmions from metafibers with subwavelength features. *Nat. Commun.* **2024**, *15*, 10141. [CrossRef]
101. Ren, H.; Jang, J.; Li, C.; Aigner, A.; Plidschun, M.; Kim, J.; Rho, J.; Schmidt, M.A.; Maier, S.A. An achromatic metafiber for focusing and imaging across the entire telecommunication range. *Nat. Commun.* **2022**, *13*, 4183. [CrossRef]

102. Zeng, C.; Luo, D.; Zhang, X.; Zhang, B.; Hu, J.; Si, R.; Liu, C.; Zhao, C.; Xie, X.; Du, Y.; et al. Planarized sidewall-integrated metafibers for enhanced evanescent field interaction via long-range resonant near-field coupling. *Laser Photonics Rev.* **2026**, e02639. [CrossRef]
103. Yang, X.; Liu, M.; Hou, J.; Li, T.; Wang, S. Topological selective non-hermitian skin effect. *Acta Phys. Sin.* **2025**, *74*, 144205. [CrossRef]
104. Liang, H.; Hou, J.; Li, T.; Wang, S. Configurable optical dirac cavity based on topological metasurfaces. *Acta Opt. Sin.* **2025**, *2*, 0709001.
105. Xiao, Q.; Ma, Q.; Ning, Y.M.; Chen, L.; Liu, S.; Zhang, J.; You, J.; Cui, J. Programmable topological metasurface to modulate spatial and surface waves in real time. *Nanophotonics* **2024**, *13*, 2141–2149. [CrossRef]
106. Li, T.; Liu, M.; Chen, C.; Li, X.; Hou, J.; Yang, X.; Wang, S.; Zhu, S. Realization of spinful metaphotonic stokes skyrmions. *J. Opt.* **2024**, *26*, 09LT01. [CrossRef]
107. Xu, L.; Curwen, C.A.; Hon, P.W.C.; Chen, Q.-S.; Itoh, T.; Williams, B.S. Metasurface external cavity laser. *Appl. Phys. Lett.* **2015**, *107*, 221105. [CrossRef]
108. Shen, Y.; Kim, A.D.; Shahili, M.; Curwen, C.A.; Addamane, S.; Reno, J.L.; Williams, B.S. THz time-domain characterization of amplifying quantum-cascade metasurface. *Appl. Phys. Lett.* **2021**, *119*, 181108. [CrossRef]
109. Zeng, Y.; Sha, X.; Zhang, C.; Zhang, Y.; Deng, H.; Lu, H.; Qu, G.; Xiao, S.; Yu, S.; Kivshar, Y.; et al. Metalasers with arbitrarily shaped wavefront. *Nature* **2025**, *643*, 1240–1245. [CrossRef]
110. Choi, D.; Zachariah, S.; Kaurav, R.; Fang, J.; Chen, J.; Laursen, B.W.; Flood, A.H.; Majumdar, A.; Alù, A.; Menon, V.M. Highly coherent organic lasing based on etch-free metasurface. *Nat. Commun.* **2026**, *17*, 906. [CrossRef]
111. Wang, M.; Lv, N.; Zhang, Z.; Chen, Y.; Si, J.; Chen, J.; Tang, C.; Yin, X.; Liu, Z.; Xin, D.; et al. Chiral orbital lasing in a twisted bilayer metasurface. *Nat. Commun.* **2026**, *17*, 2369. [CrossRef]
112. Wang, C.; Meng, C.; Mei, X.; Gui, L.; Thrane, P.C.V.; Chen, H.; Ding, F.; Xu, K.; Bozhevolnyi, S.I. MEMS-metasurface–enabled mode-switchable vortex lasers. *Sci. Adv.* **2024**, *10*, eadq6299. [CrossRef]
113. Li, T.; Xu, H.; Panmai, M.; Shao, T.; Gao, G.; Xu, F.; Hu, G.; Wang, S.; Wang, Z.; Zhu, S. Ultrafast metaphotonics. *Ultrafast Sci.* **2024**, *4*, 0074. [CrossRef]
114. Tang, H.; Huang, C.; Wang, Y.; Jiang, X.; Jin, R.; Cui, Y.; Xiao, S.; Song, Q. Dynamically tunable long-range coupling enabled by bound state in the continuum. *Light Sci. Appl.* **2025**, *14*, 278. [CrossRef] [PubMed]
115. Yoon, H.H.; Fernandez, H.A.; Nigmatulin, F.; Cai, W.; Yang, Z.; Cui, H.; Ahmed, F.; Cui, X.; Uddin, M.G.; Minot, E.D.; et al. Miniaturized spectrometers with a tunable van der Waals junction. *Science* **2022**, *378*, 296–299. [CrossRef] [PubMed]
116. Xue, Q.; Yang, Y.; Ma, W.; Zhang, H.; Zhang, D.; Lan, X.; Gao, L.; Zhang, J.; Tang, J. Advances in miniaturized computational spectrometers. *Adv. Sci.* **2024**, *11*, 2404448. [CrossRef]
117. Wang, R.; Ansari, M.A.; Ahmed, H.; Li, Y.; Cai, W.; Liu, Y.; Li, S.; Liu, J.; Li, L.; Chen, X. Compact multi-foci metalens spectrometer. *Light Sci. Appl.* **2023**, *12*, 103. [CrossRef]
118. Ji, W.; Chang, J.; Mirzaei, B.; Ridder, M.; Jellema, W.; Kao, T.-Y.; Lee, A.; Gao, J.R.; Urbach, H.P.; Adam, A.J.L. Compact metasurface terahertz spectrometer. *Laser Photonics Rev.* **2025**, *19*, 2401290. [CrossRef]
119. Fu, B.; Li, T.; Zou, X.; Ren, J.; Yuan, Q.; Wang, S.; Cao, X.; Wang, Z.; Zhu, S. Steerable chromatic dispersive metalenses in dual bands. *J. Phys. D Appl. Phys.* **2022**, *55*, 255105. [CrossRef]
120. Zou, X.; Gong, G.; Lin, Y.; Fu, B.; Wang, S.; Zhu, S.; Wang, Z. Metasurface-based polarization color routers. *Opt. Lasers Eng.* **2023**, *163*, 107472. [CrossRef]
121. Zheng, S.; Fu, B.; Zhang, H.; Wang, S. Metalens-enabled twisted chromatic dispersion. *Adv. Phys. Res.* **2026**, e00003. [CrossRef]
122. Tittl, A.; Leitis, A.; Liu, M.; Yesilkoy, F.; Choi, D.-Y.; Neshev, D.N.; Kivshar, Y.S.; Altug, H. Imaging-based molecular barcoding with pixelated dielectric metasurfaces. *Science* **2018**, *360*, 1105–1109. [CrossRef] [PubMed]
123. Wen, S.; Xue, X.; Wang, S.; Ni, Y.; Sun, L.; Yang, Y. Metasurface array for single-shot spectroscopic ellipsometry. *Light Sci. Appl.* **2024**, *13*, 88. [CrossRef] [PubMed]
124. Tang, F.; Wu, J.; Albrow-Owen, T.; Cui, H.; Chen, F.; Shi, Y.; Zou, L.; Chen, J.; Guo, X.; Sun, Y.; et al. Metasurface spectrometers beyond resolution-sensitivity constraints. *Sci. Adv.* **2024**, *10*, eadr7155. [CrossRef] [PubMed]
125. Lee, D.-G.; Song, G.; Lee, C.; Lee, C.; Jang, M. Reconstructive spectrometer using double-layer disordered metasurfaces. *Sci. Adv.* **2025**, *11*, eadv2376. [CrossRef]
126. Brackenridge, J.; Lee, J.; Tsukruk, V.V. Bridging optical and mechanical metamaterial/metasurface realms toward integrated meta-systems. *Adv. Opt. Mater.* **2026**, *14*, e03680. [CrossRef]
127. Tang, Y.; Ha, S.; Begou, T.; Lumeau, J.; Urbach, H.P.; Dekker, N.H.; Adam, A.J.L. Versatile multilayer metamaterial nanoparticles with tailored optical constants for force and torque transduction. *ACS Nano* **2020**, *14*, 14895–14906. [CrossRef]
128. Zeng, Q.; Tian, X.; Nguyen, D.T.; Li, C.; Chia, P.; Tee, B.C.K.; Wu, C.; Ho, J.S. A digitally embroidered metamaterial biosensor for kinetic environments. *Nat. Electron.* **2024**, *7*, 1025–1034. [CrossRef]

129. Zhang, L.; Bian, Y.; Wei, W.; Liao, Z.; Cang, M.; Yang, A.; Zhi, H.; Zhang, W.; Chen, M.; Cui, H.; et al. Dendrite-inspired and 3D printed multidirectional sensing piezoresistive metamaterials. *Adv. Funct. Mater.* **2025**, *35*, 2508987. [CrossRef]
130. Hong, Y.; Ye, F.; Gao, X.; Inman, J.T.; Wang, M.D. Tunable elliptical cylinders for rotational mechanical studies of single DNA molecules. *Sci. Adv.* **2024**, *10*, eadr4519. [CrossRef]
131. Peng, M.; Xiao, G.; Chen, X.; Du, T.; Kuang, T.; Han, X.; Xiong, W.; Zhu, G.; Yang, J.; Tan, Z.; et al. Optical trapping-enhanced probes designed by a deep learning approach. *Photonics Res.* **2024**, *12*, 959–968. [CrossRef]
132. Gao, G.; Shao, T.; Li, T.; Wang, S. Harnessing optical forces with advanced nanophotonic structures: Principles and applications. *Discov. Nano* **2025**, *20*, 76. [CrossRef]
133. Zhang, Y.; Li, T.; Wang, S.; Wang, Z.; Zhu, S. Polarization-dependent optical forces arising from fano interference. *Adv. Phys. Res.* **2023**, *2*, 2200048. [CrossRef]
134. Li, T.; Kingsley-Smith, J.J.; Hu, Y.; Xu, X.; Yan, S.; Wang, S.; Yao, B.; Wang, Z.; Zhu, S. Reversible lateral optical force on phase-gradient metasurfaces for full control of metavehicles. *Opt. Lett.* **2023**, *48*, 255–258. [CrossRef]

Disclaimer/Publisher's Note: The statements, opinions and data contained in all publications are solely those of the individual author(s) and contributor(s) and not of MDPI and/or the editor(s). MDPI and/or the editor(s) disclaim responsibility for any injury to people or property resulting from any ideas, methods, instructions or products referred to in the content.